# Diffuse reflectance spectroscopy-enhanced bone drill for directional feedback during spinal fusion surgery

Stijn van der Ploeg

Master thesis Mechanical Engineering

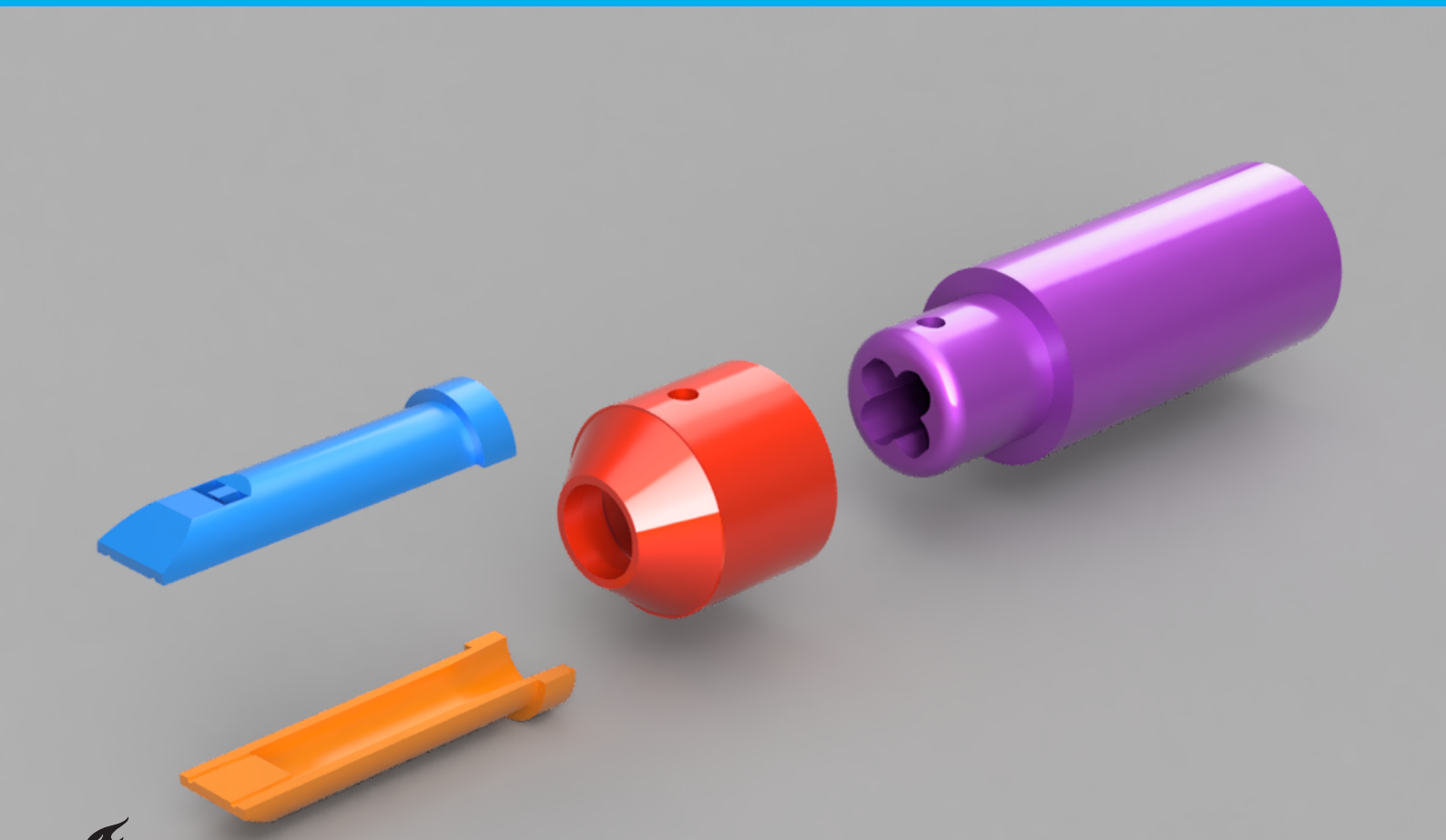

TU Delft

# Diffuse reflectance spectroscopy-enhanced bone drill for directional feedback during spinal fusion surgery

by

Stijn van der Ploeg

to obtain the degree of Master of Science
at the Delft University of Technology,
to be defended publicly on Friday April 1, 2022 at 10:00 AM.

| | | |
|---|---|---|
| Student number: | 4451759 | |
| Project duration: | May 1, 2021 – April 1, 2022 | |
| Thesis committee: | Prof. dr. J. Dankelman, | TU Delft, chair |
| | M. Losch MSc., | TU Delft, daily supervisor |
| | Dr. Ir. P. Breedveld, | TU Delft, committee member |



TU Delft

# Preface

This master thesis was written as part of the graduation from the master Mechanical Engineering Delft University of Technology. The goal of this thesis was to develop an instrument that could provide guidance based directional feedback obtain via DRS for manually drilling into a pedicle. The lumbar spine was the anatomical area of attention for the graduation project. The thesis was started in May 2021 and completed in March 2022. The work was supervised by M. Losch (TU Delft) and J. Dankelman (TU Delft). I want to specially thank my supervisor M. Losch for all her guidance and feedback during this thesis. I wish you a pleasant reading experience.

*Stijn van der Ploeg*
*Delft, March 2022*

# Abstract

The spine is an intricate and crucial part of the human body. Unfortunately, spinal conditions such as scoliosis and trauma can cause instability and deformity to the spine. Patients can experience discomfort and pain. Spinal fusion surgery is used to repair and correct severe cases. During this procedure the vertebrae are fused to prevent them from moving relative to each other, thus increasing stability. Pedicle screws and rods are used to lock the vertebrae together and bone grafts are inserted to grow the vertebrae together. The insertion of the pedicle screws is a complicated procedure where breaches of the cortical wall can occur leading to tissue damage and possible complications for the patient. To prevent breaches, guidance methods have been introduced. However, these methods have considerable disadvantages in terms of patient safety and costs. Introducing an alternative guidance method, this master thesis investigates the development of a drill that uses diffuse reflectance spectroscopy (DRS). DRS is a spectroscopy method that uses diffuse reflection to determine the structural and chemical properties of a biological sample. By differentiating cortical and cancellous bone based on their fat content, directional feedback is provided to guide the user during the drilling of the pedicle.

In this work, a drilling prototype was developed that uses DRS to provide directional feedback. The prototype uses integrated optical fibres to sense in two different directions: along the drilling direction and at a 90°angle to the drilling direction. This allows the device to sense the surrounding volume and provide feedback on the type of bone the drill encounters.

A 3D Monte Carlo RTE solver, *MCMatlab*, was used to simulate photon transport inside biological tissue. Core-to-core distances larger than 1 mm were investigated to find if the corresponding look-ahead would increase distances as well as different fibre configurations for a prototype.

Multiple design concepts were proposed and assessed. A prototype was made and tested on a 2-layered bone phantom. The results indicated a frontal look-ahead distance of 3.6 mm for a 4 mm core-to-core distance as well as a 1.5 mm sideways look-ahead distance for a 1.5 mm core-to-core distance.

The prototype provides a proof of concept that DRS can be integrated into a drill in such a way it can provide directional feedback. Although results are promising, improvements can still be made in the collection of data to provide consistent results for directional feedback.

# Contents

# 1 Introduction

A large amount of spine surgery related procedures is performed each year. In 2017, it was estimated that worldwide around 5.2 million spinal procedures were performed[1]. Moreover, a forecast suggests that this number will increase to a total of 7.6 million in 2022. These spinal procedures include spinal decompressions, fusion surgeries, disc replacements and deformity corrections for conditions such as scoliosis. During spinal surgery complications can arise such as the misplacement of hardware, for example pedicle screws. To decrease the number of complications, guidance methods have been introduced to help the surgeon and increase accurate hardware placement. Image-based guidance methods such as fluoroscopy and computed tomography have been used to decrease the breach rates during pedicle screw placement [2]. However, these methods pose a risk to the patient and medical personnel as they make use of ionizing radiation which is harmful to the human body.

New methods are being investigated that could be adopted for the use of guidance during the placement of hardware such as pedicle screws. A promising new method that uses diffuse reflectance spectroscopy has been proposed. Research has indicated that the method can be used to detect cortical bone [3]. Therefore, it is possible to make a device that can sense the cortical wall and provide feedback to prevent breaches. Such a device could help in lowering the amount of surgical complications, increasing patient comfort and saving costs. However, such a device does not exist yet. This thesis investigates the design of such a device. The following sections are used to provide background information on this topic.

## 1.1. Background information

### 1.1.1. The spinal anatomy

The spine is located along the back of the human body. The spine forms the backbone of the human body and is an intricate structure consisting of bone, muscle, nerves and connective tissue such as ligaments and tendons. The spine is built up out of alternatively stacked vertebrae and discs. The spine has 24 vertebrae located in the upper three spinal regions, namely, the cervical, thoracic and lumbar regions. The bottom two areas are the sacrum and coccyx, or tail bone. These two regions consist of several small bones that fuse as one grows older. The build-up of the spine is shown in Figure 1.1. Each of the coloured areas represents a section of the spine containing vertebrae.

A vertebra can be divided into five main parts: the spinous process, lamina, two pedicles, and vertebral body. The latter four parts surround the vertebral foramen. The vertebral foramen surrounds the spinal cord and protects the spinal cord on all sides from external trauma. This protection is vital as the spinal cord consists of nerves running from the brain to the body. The spinal cord's function is to

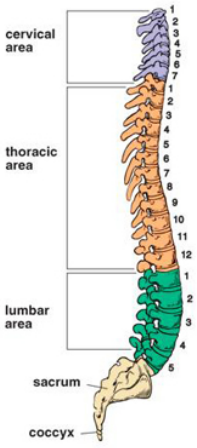


Figure 1.1: The build-up of the spine [4]. Each number represents the corresponding vertebra in its respective area.

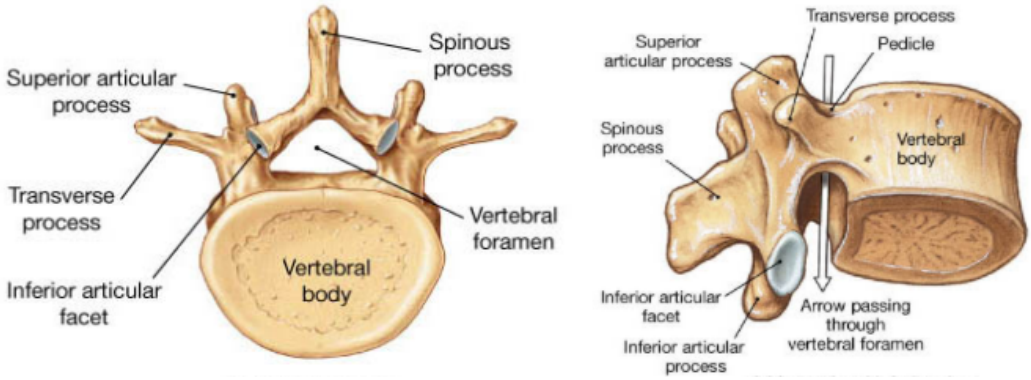


Figure 1.2: On the left, an inferior view of a lumbar vertebra. On the right, an inferior and lateral view of a lumbar vertebra (adapted from [7]).

carry signals from the brain to the body and vice versa [5]. The transverse processes attached to both sides of the vertebra act as attachment points for muscles and ligaments [6]. An example of a lumbar vertebra is shown in in Figure 1.2.

Located between each vertebrae pair is an intervertebral disc, as shown in Figure 1.3 in purple. The intervertebral disc consists of fibrocartilage and has multiple functions. It acts as a shock absorber for the spine and prevents the vertebrae from touching during movement, thus preventing wear. In addition, the discs allow for slight movement between the vertebrae, giving the spine its flexibility and enabling the spine to rotate [8].

Spinal instability is often used to describe a range of conditions in which the degeneration of a disc leads to an inability to support the body's weight along that part of the spine [9]. The degeneration of the disc allows for more motion between two vertebrae than normal and can cause an imbalance in the spine, thus further deteriorating the disc. Other conditions range from external ones such as trauma to the spine to congenital ones such as scoliosis. For some cases of scoliosis, a deformity in the spine can develop at a later stage in life. The extreme deformation and/or instability of the spine can lead to the need for a correction. This is done by performing spinal fusion surgery.

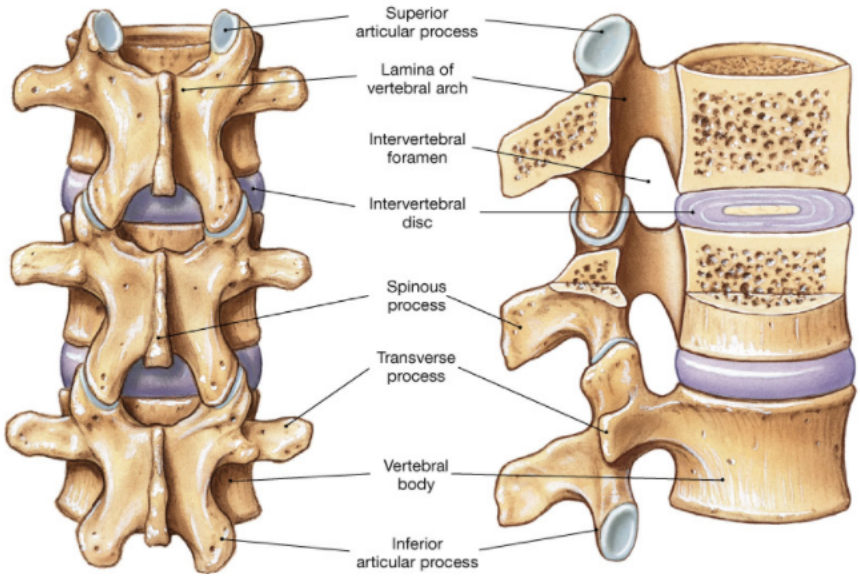


Figure 1.3: A posterior (left) and a lateral cross-sectional view (right) of a section of spine (adapted from [7]).

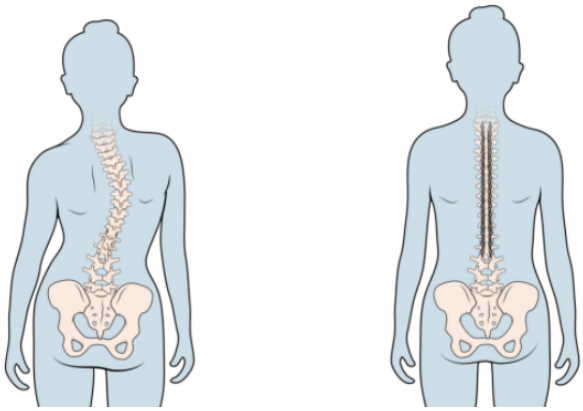

Figure 1.4: On the left, the spine is curved in an S-shaped form, indicating scoliosis. On the right, the spine is straightened after fusion surgery. Rods and pedicle screws are placed on both sides of the spinous process to fixate and stabilize the spine. (Illustration adapted from childrenshospital.org.) [10]).

### 1.1.2. Spinal fusion surgery

Spinal fusion surgery is a procedure performed to stabilize the spine and prevent further deterioration of the spine. During spinal fusion surgery, the goal is to fixate and to avoid movement between the affected vertebrae. By taking away the mobility of the vertebrae, pain can be reduced. For scoliosis, the spine is straightened using hardware before the vertebrae are fixated. An example of this can be found in Figure 1.4. The general procedure for spinal fusion surgery consists of the following steps: first, the relevant area of tissue above the spine is opened up to obtain access to the spine. The size of the incision depends on the type of surgery that is performed. A large incision is made to separate the overlying muscle and tissue for invasive surgery. For minimally invasive surgery, small incisions facilitate the entry of the instrumentation to the surgical site [11].

Next, after the vertebrae of interest are identified, the harder cortical bone preventing access to the pedicles is removed to reach the softer cancellous bone beneath. Depending on the procedure, holes are pre-tapped through both pedicles into the vertebral body before pedicle screw insertion, or self-tapping screws can be used [12]. The number of vertebrae that are fixated depends on the severity of the condition that needs to be corrected.

The pedicle screws are inserted into the vertebral body as this can add up to 20% more fixation strength[13]. However, the largest part of the fixation strength is attributed to the screw fixation inside the pedicle[13]. This strengthens the notion, that accurate pedicle screw placement is a crucial part of the spinal fusion surgery. If the screws are not placed correctly, the hardware can come loose due to the cyclical loading it experiences due to the patient's movement [14].

When the insertion of the pedicle screws is completed, rods are connected to the pedicle screws along the spine, as shown in Figure 1.5. After removing parts of the degenerated discs, bone grafts are placed in between

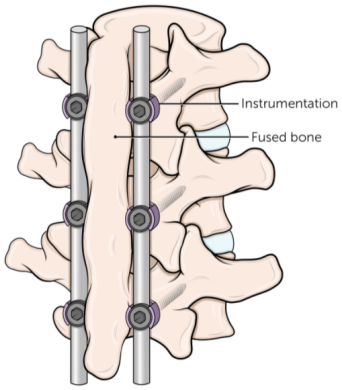


Figure 1.5: A section of the spine on which fusion surgery has been performed. Rods are connected to the pedicle screws on both sides of the spinous process to fixate the vertebrae. (Illustration adapted from childrenshospital.org, all rights reserved.)

the affected vertebrae. The bone grafts grow and thereby fuse the vertebrae. This fixates the vertebrae to each other and prevents movement relative to each other.

It should be noted that the aforementioned steps can be performed in a different sequence depending on the spinal condition. Deformities of the spine can make it harder to reach the affected disk due to the positioning of the vertebrae. Such cases would warrant early hardware placement in the procedure to gain better access to the disc. For other cases such as spinal instability, the disc can be removed first to alleviate the pressure before the hardware and bone graft are placed to stabilize and fuse the vertebrae [15].

### 1.1.3. Pedicle screw placement

**Conventional method**

The placement of the pedicle screw is an important step in a spinal fusion procedure. During this step, there is the risk of breaching the cortical wall of the pedicle or vertebral body, thereby damaging the surrounding tissue, which contains nerves and blood vessels. A breach can lead to post-surgical complications and could warrant reoperation to correct the difficulties.

The conventionally used method for the placement of pedicle screws is the free-hand technique. The surgeon drills and places the screws by hand. By relying on the bony landmarks of the spine, such as the transverse and spinous processes and the difference in density of the cortical and cancellous bone inside the pedicle, surgeons can find the correct trajectory for the insertion of pedicle screws [15], [16]. Gelalis et al. (2012) reviewed the accuracy for pedicle screw placement using the free-hand technique and reported screw displacements ranged between 5% and 41% [17].

To lower screw displacement rates, guidance systems are used during spinal fusion surgery to provide feedback to the user and prevent breaches of the cortical walls. The guidance systems rely on different principles to obtain the data on the anatomy. Guidance methods can be divided into imaging-based and non-imaging-based methods [15]. The imaging-based methods provided imaging of the surgical site to the user as feedback. Non-imaging-based methods provide other types of feedback to its user, such as sound or other types of visual feedback.

**Imaging-based guidance**

*Fluoroscopy*

Fluoroscopy is a type of radiography that is used intraoperatively. It utilizes ionizing radiation to provide imaging of the relevant anatomy. The images are directly processed and presented to the relevant personnel during the operation. This has the added benefit that possible breaches can be directly detected and repaired if necessary. This prevents complications from arising later on.

Using a C-arm machine, 2D images can be taken from the anatomy at different angles. This helps verify the correct placement of the instrumentation during spinal fusion surgery. Research reported breaches rates for pedicle screw placement using fluoroscopy to be between 18 and 31% [18] [19]. Although the use of fluoroscopy is widely adopted during spinal fusion surgery [20], the use of ionizing radiation is still a significant disadvantage. Not only is ionizing radiation damaging to the patient, it is also a safety hazard for the surrounding medical personnel.

*Computed Tomography*

Computed Tomography (CT) is also an imaging method based on ionizing radiation. By rotating the radiation source and detector around the patient, cross-sectional slices of the body are imaged separately using either a fan- or cone-shaped beam. These images can either be used in 2D, or a 3D model by combining the images' data.

CT in combination with a dynamic referencing array and markers on the patient's body can be used to overlay the CT images and 3D model on top of the actual anatomy together with the instrumentation during the operation. This allows the surgeon to have a real-time view of the position and orientation of their tools to the anatomy. Chan et al. (2017) reported breach rates between 1.5% and 22.3% when CT was used to guide pedicle screw placement [2].

The CT images are made preoperatively, which means that it is possible for the anatomy in the images to deviate from the actual anatomy during the operation due to the moving of the patient. However, as the images are made preoperatively, medical personnel is not exposed to radiation. Another disadvantage is the cost of CT machines compared to other forms of imaging such as fluoroscopy.

*Sonography*
In sonography, imaging is done using an ultrasound probe. The ultrasound probe is placed on the anatomy of interest, and ultrasonic waves are sent into the body. The ultrasonic waves interact with the different tissues that make up the anatomy and are partly absorbed and reflected. The probe collects the reflected sound waves, also called echos, and processes them into images.

Compared to fluoroscopy or CT, ultrasound has some significant benefits. Ultrasound uses sound waves, which are not harmful to the patient and the user. Furthermore, the equipment needed to make ultrasound is relatively cheap compared to the other imaging methods using ionizing radiation and can easily be used inside an operation room due to its size. However, the use of ultrasound for guidance purposes has some shortcomings. The image quality for imaging hard tissues is low and experience is needed to distinguish and identify the relevant anatomy.

**Non-imaging-based guidance**
Not many options for non-imaging-guidance exist that can be used during pedicle screw insertion. However, a handheld device called the Pediguard (Spineguard, USA) makes use of conduction to help the user anticipate and notice a breach of the cortical wall. It provides audible feedback, which acts as the guidance for the user.

The device has a sharp tip to penetrate the cancellous bone inside the pedicle. The difference in conductivity of cancellous and cortical bone is used to differentiate the two types of bone and, therefore, the device's relative position inside the pedicle.

If the Pediguard enters the cortical bone, the device produces a different sound to let the user know that the device's tip has reached the cortical bone. In the case of a cortical breach, blood from the surrounding tissue will flow through the breached cortical bone. The occurrence of blood in combination with the different conductivity of the cortical bone is used to notify the user of a potential breach. The occurrence of blood can be noticed due to its different conductivity compared to the two types of bone.

In terms of optical guidance, diffuse reflectance spectroscopy has shown promising results in breach detection for pedicle screw placement[15]. However, no commercially available options for use during spinal fusion surgery exist yet. This creates potential for the development of a new surgical guidance tool for pedicle screw insertion.

### 1.1.4. Diffuse reflectance spectroscopy
Diffuse reflectance spectroscopy (DRS) is a non-invasive optical spectroscopy method used to determine biological tissue structure and chemical properties. The technique uses a light source with a known emission spectrum to send photons into a tissue sample. After the light has interacted with the sampled tissue, it is again collected to study the absorption and emission of the light. In this case, light refers to a broader spectrum of electromagnetic radiation and not only the visible spectrum for humans. The principle of DRS is shown in Figure 1.6.

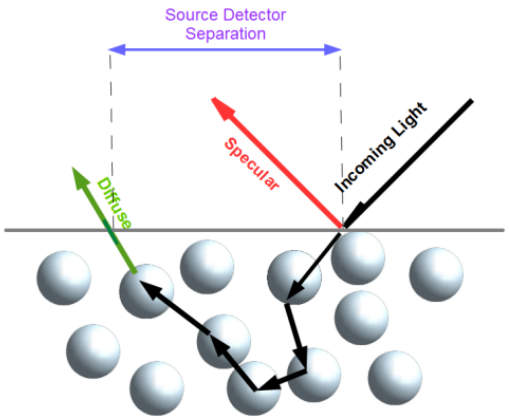


Figure 1.6: Specular and diffuse reflectance using DRS. The light from the source enters the tissue at the black arrow. Inside the tissue, the light scatters. The light that escapes the tissue is diffuse reflected light and is collected again at a specific source distance. [21].

Light that hits the sample's surface either refracts or is specular reflected. The light suffering specular reflection is directly reflected off the sample's surface; thus, no information is obtained from the composition of the sample [22]. Therefore, this type of reflected light is not relevant for DRS.

Light that is refracted into the sample is either absorbed or scattered. As the photons pass through the tissue and interact with the molecules which make up the tissue, molecules can absorb the energy of the photons. When this occurs, the energy level of the molecule jumps from a lower energy ground state to a higher state of excitation [23].

A molecule only absorbs the energy of a photon with a wavelength whose energy level corresponds to the energy that is needed for the molecule to jump to its excited state [23]. Therefore, as long as no photons with a suitable energy level are available, the molecule will not absorb energy. This means that depending on the sampled tissue, only certain wavelengths of light are absorbed. As the molecule returns to an energy ground state, depending on the type of scattering, elastic or non-elastic, light of the same or a different wavelength is emitted. For DRS, light of the same wavelength is used.

The sampled tissue is not homogeneous but contains various components, each with a different refraction index. Therefore, the refracted light is scattered in multiple directions inside the tissue, part of which is emitted from the tissue. The diffuse reflected light is collected and quantified. This results in a spectrum visualizing the diffuse reflectance as a function of a wavelength.

**Applications**

DRS can be used to distinguish tumorous tissue from healthy tissue [24], [25]. Swamy et al. (2019) showed that it is possible to use DRS as a tool to detect cortical breaches. They did DRS measurement using optical fibres integrated into a needle. They measured significantly higher fat content in the cancellous bone compared to the cortical bone. This difference in the fat content of cancellous and cortical bone can be used to differentiate the two types of bone. Therefore, a DRS probe can potentially be used to provide guidance during the drilling into the pedicle and let a user know in which type of bone they are drilling.

To be able to use DRS in the area of interest, optical fibres can be used to emit and collect light. Due to the size of the optical fibres, it is possible to integrate them into a drill without increasing the size of the tool [26]. This could result in a device similar to the size of Pediguard. Another significant benefit of DRS over other imaging methods is the type of wavelengths required to operate. DRS utilizes non-ionizing electromagnetic radiation to obtain data. This type of radiation is harmless to tissue. Therefore, DRS is safe for both the patient and the medical personnel handling the equipment. This does come at the cost of not being able to provide an image of the relevant anatomy and thus an overall view of the situation.

## 1.2. Problem statement

As mentioned before, DRS has shown promising results for providing guidance based on fat detection inside the bone [3]. Probes for DRS already exist, and prototypes have been made by integrating optical fibres into drills [26]. However, these instruments can only sense in one direction and provide feedback regarding the bone directly in front of the device. This type of feedback is not enough to actively redirect the device in case of an imminent breach. Therefore, directional feedback needs to be acquired inside the pedicle to guide the user during drilling into the pedicle. If such feedback could be provided to the user, it would be possible to actively avoid breaches by redirecting the device in case of an imminent breach. However, currently, no solutions exist that allows a drill to sense the cortical wall using DRS and provide directional feedback to the user to prevent perforation of the cortical bone. Such a solution could reduce accidental breaches as the user would know in advance that they need to adjust the drilling direction.

## 1.3. Goal and structure

This thesis aims to design a drill with integrated DRS that can provide directional feedback for guidance. The instrument needs to detect the cortical wall when the instrument is on an intersecting path with the cortical wall. A proof of concept is built that uses diffuse reflectance spectroscopy (DRS) to sense the surrounding tissue using integrated optical fibres. The directional feedback provided by DRS is used to avoid perforations of the cortical wall. Simulations are done to determine relevant design parameters systematically. Chapter 2 explains the design requirements to which the prototype needs to adhere and their rationale. Chapter 3 reports the simulations done to determine the core-to-core distances for the optical fibres and the configuration of the individual fibres. In addition, the results of the simulations are validated based on an experiment performed using a multi-fibre probe. Chapter 4 elaborates on the design process and concept generation.

The different concepts are evaluated and scored to determine a suitable design for a prototype. Chapter 5 reports on the testing of the prototype. Chapter 6 discusses the results obtained during this thesis. Limitations are stated, and recommendations for future research are made. Lastly, Chapter 7 provides the conclusion for this thesis.

# 2

# Design Requirements

## 2.1. Introduction

Studies looked into the detection of cortical bone for breach detection [3], [27], [28] while others have tested a prototype with integrated optical fibres to detect the cortical boundary in bone [26]. However, these studies did not look at using this detection to obtain directional feedback inside the bone. Therefore, a list of design requirements is drafted to ensure that a final prototype is up to the required standard and can be tested. In this list, two types of requirements are defined for the instrument. The first type focuses on the guidance and feedback of the device. The second type is the requirements regarding the hardware. During the prototype testing, these design requirements are to be validated.

The device is seen as a medical device which means that its design should adhere to the guidelines for medical devices (IEC60601-1). However, the purpose of this prototype is to give a proof of concept that DRS can be used to obtain directional feedback and thus be used to guide spinal surgery. Therefore, requirements for medical equipment were not strictly considered during the design phase. Material choices were considered in the discussion.

## 2.2. Guidance requirements

The device needs to provide directional feedback from inside the bone, in this case, the pedicle and vertebral body. DRS is the method used to obtain the surrounding tissues' reflectance spectra. Therefore, the transport of the light from the source to the instrument is essential. Optic fibres are a convenient and often used way to transport light in the medical world [29]. Fibre optics provide multiple benefits: first, optical fibres are commercially available and, therefore, easily obtainable. Moreover, the diameter of the available optical fibres is small. The optic fibres used in this thesis have a diameter of 200 µm, which helps to keep the size of the instrument compact. Thirdly, the fibre optics cables can transport light efficiently over short distances without amplifying the signal [30]. Over long distances, the intensity of the light in the optic cable decreases. However, this decrease in intensity for the current optic fibre is 10 dB/km at 808 nm [31], while the total length used for this project will be no more than 2 m. Therefore, the intensity loss of the light in the cable is negligible. The specifications for the optical fibres used during this thesis can be found in Table 2.1.

Table 2.1: The specifications of the optical fibres used during this thesis.

| **Specifications of TECS Step-Index, Multimode Fiber (by Thorlabs)** | |
|---|---|
| Wavelength Range (Low OH / high OH) | 400 - 2200 nm / 250 - 1200 nm |
| Core / Cladding | Pure Silica / Fluorine-Doped Silican |
| Coating | TECS Hard Fluoropolymer |
| Buffer | Tefzel |
| Operating Temperature (Tefzel Buffer) | -60 to 125 °C |
| Numerical Aperture (NA) | 0.22 ± 0.02 |
| Max Attenuation @ 808 nm | 10 dB/km |
| Max bending radius (short term/ long term) | 12 mm / 24 mm |

Table 2.2: The guidance requirements for the proposed device.

**Guidance Requirements**

| *Requirement* | *Rationale* | *Value* |
|---|---|---|
| The drill should be able to detect the pedicle wall 2.0 mm in front of it. | By inserting the drill too far, the cortical wall of the bone body. The LAD was set at a minimum of 2.0 mm with an accuracy of 0.5 mm | Forward LAD ≥ 2.0 mm, an accuracy of 0.5 mm |
| The drill should detect the bone/pedicle wall sideways at a 1.0 mm distance. | If the fibres can sense the cortical wall surrounding the instrument, a user can maintain a constant distance to the wall. Therefore, the LAD for sideways sensing was set at a minimum of 1.0 mm with an accuracy of 0.5 mm. | Sideways LAD ≥ 1.0 mm, accuracy of 0.5 mm |

The device needs to detect the tissue along its path inside the pedicle during spinal surgery. The instrument needs to sense the distance to the surrounding pedicle walls to achieve this requirement. A user can then use this feedback to obtain the orientation of the drill in the pedicle. If the drilling direction intersects with the pedicle walls, the user can adjust the drill direction to avoid penetration of the pedicle wall.

A sensing volume around the drill is needed to detect the cortical wall. This need can translate into two requirements. The first requirement is to sense ahead of the device to know if the user should stop drilling. The drill should sense sideways for the second requirement to detect the distance to the surrounding cortical walls inside the pedicle. Sensing forwards and sideways establishes a sensing volume that detects the cortical walls of the pedicle. The optical fibres must be configured inside the instrument to detect this volume. The simulation results determined the respective configurations during this thesis. Therefore, the design incorporates two frontal facing fibres and two sideways facing fibres. The reasoning behind this configuration is explained in section 3.6.

Eventually, medical personnel can use this device for medical purposes. The accuracy of the feedback is crucial for the user to rely on the instrument for guidance. Therefore, the information acquired using DRS should be able to measure the distance to the surrounding cortical bone with an accuracy of 0.5 mm. Table 2.2 contains the guidance requirements to which the device should adhere.

## 2.3. Dimensional Requirements

For size reference, the upper lumbar vertebrae are used as they are larger overall than their counterparts in the cervical and thoracic spine. Referencing the lumbar vertebrae allows for more margin in the drill diameter during the design phase than the other vertebrae types. An example of a lumbar vertebra is shown in Figure 2.1. The lower vertebrae in the spine are the most frequently affected by abnormalities and often receive implants, such as pedicle screws. Zhou et al.(2000) looked into the geometrical dimensions of the lower lumbar vertebrae as the anthropometric data sets for these vertebrae were incomplete [33]. The research obtained more accurate anthropometric data and enlarged the existing lumbar vertebrae data sets. Zou et

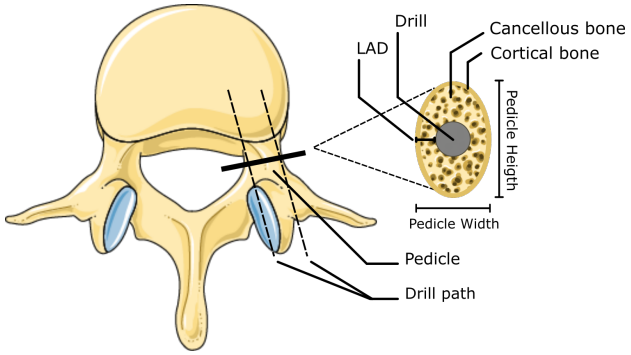


Figure 2.1: On the left a lumbar vertebra, where the dotted line shows the drill path through the pedicle. Adapted from [32]. On the right a cross-sectional view of the pedicle is shown along with the general position of the drill.

Table 2.3: The dimensional requirements for the proposed device.

**Dimensional Requirements**

| *Requirements* | *Rationale* | *Value* |
|---|---|---|
| The maximum drill diameter is 6 mm | Enough bone should be left in the pedicle for a screw to be properly secured. By leaving enough bone, the pedicle has the strength to resist the dynamic forces the screw experiences. Zhou et al. (2000) found that, on average, the female lumbar pedicle (L3) has a mean diameter of around 8.7+-1.9 mm [33]. | Instrument diameter ≤ 6.0 mm |
| The drill needs to be equal to or longer than 15.0 mm | The drill should reach the bone body behind the pedicle. Therefore, the drill length is set at a minimum length of 15.0 mm [34]. | Length ≥ 15.0 mm |

al.(2000) found that, on average, female lumbar vertebrae are smaller, with an average width of 8.7 mm ±1.9 mm. Therefore, a maximum diameter of 6 mm was set for the diameter of the instrument. This diameter ensures that an individual can use the instrument on most adult male and female patients during spinal surgery (children's pedicle diameter not included). This instrument diameter also excludes its use on patients with pedicles smaller than 6 mm. However, the goal is to provide a proof of concept for the guidance a manual drill with integrated optics could provide. Therefore, to constrain the prototype's design to reasonable dimensions, the anatomical geometry of pedicles is taken into account. The geometry of the lumbar vertebra constrains the diameter of the instrument. The diameter of the drill is limited to the diameter of the pedicle. The elliptical pedicle's height is larger than its width [33], as indicated in Figure 2.1.

The length of the device does not have an impact on the sensing performance of the device. However, this dimension needs to be taken into account, considering that the instrument will have to pass through the pedicle to reach the bone body of the vertebra. Gstoettner et al.(2011) did a reliability assessment of computed tomographic 3D measurement of pedicles in scoliosis. They measured the vertebrae of scoliosis patients between 9 and 24 years old (mean age 14.9 years). They measured the pedicle length by taking the distance between the dorsal edge of the vertebral body to the articular processes. The data indicated that the average pedicle length for the lower lumbar vertebrae (L5) was 7 mm [34]. However, one of the individuals was measured to have a pedicle length of 11.7 mm. To include longer pedicles, the minimum insertion length of the device is set at 15 mm. The above mentioned dimensional requirements are shown in Table 2.3.

## 2.4. Hardware Requirements

During insertion of the device, it will experience forces that could bend the device. Bending during the device's insertion into the pedicle can be problematic as it could cause the instrument from deviating from its course. Although the feedback provided by the device should enable the user to correct the course, this cannot be assumed. Therefore, the prototype should not have a deviation of more than 0.5 mm from its own central axis.

The device should have the ability to create holes in cancellous bone. The cortical bone above the pedicle is too hard to penetrate. Thus, the cortical bone is chiselled open. The cancellous bone beneath the cortical bone is softer than cortical bone. Therefore, it is possible to create a hole by applying force with a sharp object. An example of such an object is the Pediguard (Spineguard SA France) which creates holes through the pedicle similarly. The instrument needs to have a slanted tip to make drilling feasible. A point angle of 90° and 118° is used in drill bits for the spine. The point angle is defined as: "the angle formed by the projection of the cutting edges onto a plane passing through the longitudinal axis of the drill-bit" [35]. Therefore, a maximum of 90° is set for the point angle of the instrument.

The optical fibres that will be used have a maximum bending limit, which means that the fibres cannot be bent beyond a certain radius. The optical fibres used for this thesis have a short term bending radius of 26.4 mm and a long term bending radius of 52.8 mm. If the fibre exceeds this radius, damage is likely to occur. The short term bending radius can be used while installing the fibre, but an installed fibre should adhere to the long term bending radius. This instrument is used for more extended periods; the long term bending radius needs to be met. Table 2.4 contains the hardware requirements to which the device should adhere and is shown on the next page.

Table 2.4: The hardware requirements for the proposed device.

**Hardware Requirements**

| *Requirements* | *Rationale* | *Value* |
|---|---|---|
| The drill needs to be stiff in the axial direction, with a deflection < 0.5 mm | The forces applied to the device could result in bending the instrument. The forces could cause the instrument to deviate from the correct pat, thus requiring redirecting. A high axial stiffness can prevent this and make it more convenient to drill straight. Furthermore, this will prevent the drill from buckling and breaking inside the pedicle. | Deflection < 0.5 mm |
| The drill can penetrate cancellous bone by hand | The use of an automated device for drilling in the spine would complicate the design. Non-automated handheld devices such as the Pediguard (Spineguard SA France) and Lenke probe are used during spinal surgery. Therefore, the prototype will also be a handheld device that is manually operated. Proper penetration of the cancellous bone can be assured with a tapered tip. A minimum tip angle of 90° needs to be used based on bone drills [35]. | Tip angle > 90° |
| Optic fibres should not be subjected to a bending radius smaller than 52.8 mm. | The optical fibres are fragile and prone to breaking when experiencing bending smaller than their minimum bending radius. For these fibres, that is 26.4 mm for the short term and 52.8 mm for the long term bending. Efforts should be made to ensure these fibres' careful and stress-free handling. | Bending radius ≥ 52.8 mm |

## 2.5. Miscellaneous Requirements

The optic fibres integrated into the instrument are relatively fragile and thus prone to breaking when subjected to bending and stress. Therefore, the optical fibres should be handled with care to avoid damaging them. The use of strain relief on the fibre tubing can absorb and negate forces that could harm the integrity of the optic fibres.

Furthermore, the instrument should be produced out of medically approved materials, for example, stainless steel. If the design does not consider such materials, it could be problematic. This requirement is added as this prototype could eventually become a medical device. However, this requirement is not strictly adhered to as it does not add value to the proof of concept. Table 2.5 contains the miscellaneous requirements to which the device should adhere.

Table 2.5: The miscellaneous requirements for the proposed device.

**Miscellaneous Requirements**

| *Requirements* | *Rationale* |
|---|---|
| The device should have an integrated strain relief. | The optic fibres are fragile and prone to breaking. An integrated strain relief applied to the fibre tubing can absorb forces to protect the optical fibres. |
| The drill should be made out of stainless steel. | Medical devices cannot use all materials. Therefore, stainless steel was chosen as this is a bio-compatible material often used in surgical devices and implants. This material can be sterilized, making the drill reusable. |

# 3

# Diffuse reflectance spectroscopy simulations

## 3.1. Introduction

For DRS, to sense the volume of the bone surrounding the device, optical fibres are necessary. Therefore, these are mounted into the instrument. However, the distance between the emitting and collecting fibre, the core-to-core distance, influences the distance that can be sensed ahead. This is called the look-ahead distance (LAD). Therefore, the necessary core-to-core distance and the optical cables' configuration must be determined before a prototype design is made. A search was performed to find literature regarding the look-ahead distance inside cancellous bone concerning the core-to-core distance. The search investigated the change of LADs as core-to-core distances were increased.

Multiple papers reported using DRS to help detect cortical breaches by detecting changes in lipid concentrations [27], [36]. However, none of these papers looked explicitly into the relation between the core-to-core distance and the LAD. Li et al. (2014) did look into the LAD using a core-to-core distance of 0.2 mm. They obtained a LAD of around 0.6 mm, consistent with their simulation and experimental validation [28]. Nevertheless, no relation was given that predicts the LAD for a certain core-to-core distance. In addition, Li et al. (2014) used only a core-to-core distance of 0.2 mm but did not look into the effect of a larger core-to-core distance on the LAD. In another study, Duperron et al. (2019) obtained a LAD between 0.25 mm for automated drilling of holes and a 1 mm LAD when drilling by hand. The core-to-core distance used was 1.3 mm. The relation between the LAD and core-to-core distance in both studies is inconsistent. The literature search did not find other correlations for higher core-to-core distances and the LAD inside the cancellous bone. Therefore, simulations were run to see if larger core-to-core distances would result in higher LADs.

Simulations were done to gain more insight into the LAD inside cancellous bone due to the more considerable core-to-core distances ( $>1$ mm). However, simulations can only replicate DRS to some extent; thus, the results require validation. Therefore, a validation experiment is done to check the simulation results. The advantage of simulating to determine the LAD for different core-to-core distances is its flexibility when choosing different fibre configurations. Testing a new design or idea does not require one to make a setup and experimentally obtain the data.

## 3.2. Monte Carlo-based photon simulations

The behaviour of the light inside a biological material needs to be modelled to simulate DRS. Light consists of photons that can be individually modelled. Therefore, the path and scattering of the individual photons inside a medium can be calculated. The gold standard for simulating this type of complex scenario is Monte Carlo based-simulations [37]. Monte Carlo based-simulations use a large number of random repeated independent computations to generate a numerical result [38].

A software package called MCMatlab was used to run the Monte Carlo-based simulations. MCMatlab is open-source software that requires no C knowledge, often required when running Monte Carlo simulations. The software is run using MATLAB, where it operates a 3D Monte Carlo RTE solver to simulate the path of photons throughout the material [39].

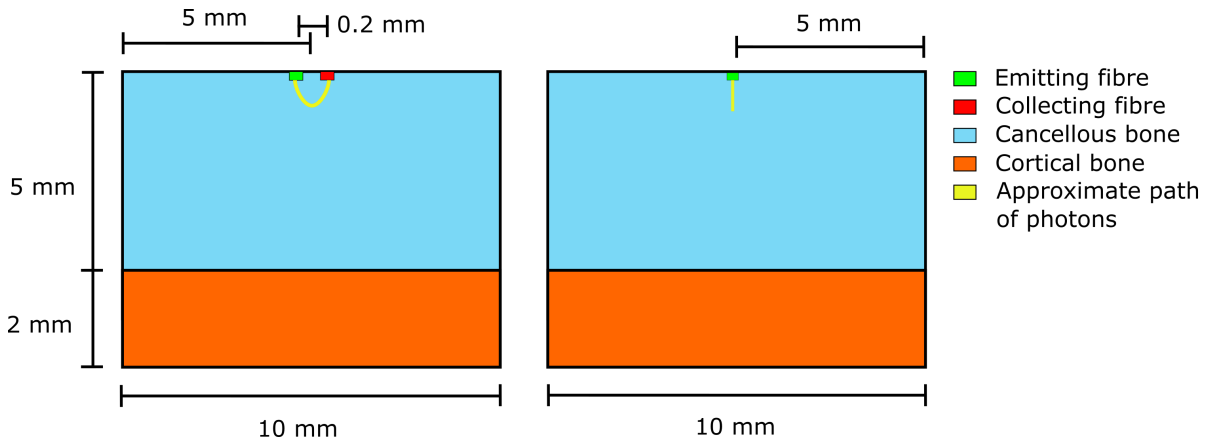


Figure 3.1: A visualisation of simulation volume. On the left a front view of the cuboid. On the right, a side view of the cuboid.

Li et al. (2014) found that an alarm threshold can be deduced for pedicle screw insertion based on Monte Carlo simulations. The study looked into the detection of a cortical layer [28]. However, they only used a core-to-core distance of 200 microns and did not show a relation for a larger core-to-core distance and its influence on LAD. Therefore, their results could not be used the determine the necessary core-to-core distance. This study was used to see if the software worked as intended. Furthermore, the method used in this simulation can be adjusted to investigate larger core-to-core distances.

## Method

This simulation included all the parameters reported in Li et al.(2014). The parameters are reported in Table 3.1. Li et al. (2014) did not report the width and length of their simulation volume. Therefore these parameters were set to 1 cm. This should be enough as the height of the volume is set to 0.7 cm and is the direction of interest. The number of bins was calculated with the reported voxel size and the parameters for the simulation volume.

The simulation volume was separated into two layers. The simulation started with a top layer that resembled cancellous bone with a thickness of 5 mm. The bottom layer resembled cortical bone and was 2 mm thick. The material properties of both layers are reported in Table 3.1. At each new depth, measurements were done using 1e6 photons with a wavelength of 690 nm. During the simulation, the simulated fibres could not enter the simulation volume. Therefore, the bottom layer was moved step wise upwards in steps of 0.2 mm. When the thickness of the cancellous layer reached 1 mm, the step size was lowered to 0.1 mm to obtain a higher resolution for the LAD. During the simulation, simulation volume was kept constant. The positioning of the emitter and the collector are shown in Figure 3.1.

Table 3.1: The simulation parameters used by Li et al. (2014) [28].

| **Parameters used for test simulation** | |
|---|---|
| *Amount of photons* | 1e6 photons |
| *Wavelength light* | 690 nm |
| *Emitter properties* | Pencil beam |
| *Collector diameter* | 200 microns |
| *Core-to-core distance* | 200 microns |
| *Material properties* | *Top layer*: $\mu_s$ = 17.23 $cm^{-1}$ and $\mu_a$ = 0.41 $cm^{-1}$<br>*Bottom layer*: $\mu_s$ = 12.02 $cm^{-1}$ and $\mu_a$ = 0.21 $cm^{-1}$<br>n = 1.38 (index of refraction), g = 0.9 (anisotrophy factor) |
| *Simulation volume* | 10 mm x 10 mm x 7 mm (w x d x h). |
| *Nr. of bins* | x-direction: 50<br>y-direction: 50<br>z-direction: 140 |

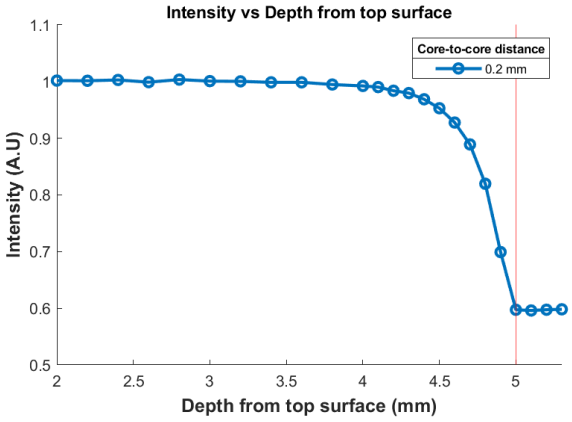


(a)

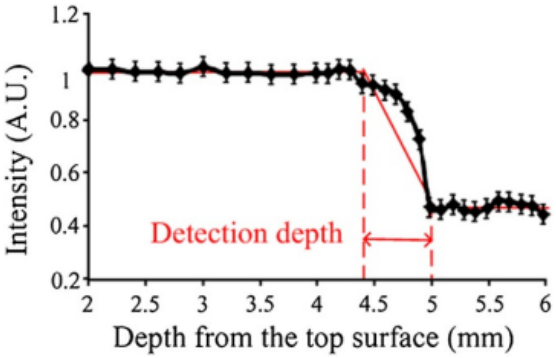


(b)

Figure 3.2: In (a), the figure shows the results obtained from the test simulation. The red line indicates the boundary between cancellous and cortical bone. In (b), the results of the simulation done by Li et al. (2014) [28].

## Results

The intensity was calculated by taking the number of detected photons and dividing it by the total amount of simulated photons. The resulting intensities are shown in Figure 3.2a. The simulation result by Li et al. (2014) is shown in Figure 3.2b.

As the distance between the light source and the cortical layer decreases and light starts to enter the cortical boundary, the overall intensity of the collected light begins to decrease as well. After the light source enters the cortical layer, the intensity of the collected light becomes constant again. Li et al. (2014) determined the LAD by subtracting the boundary depth by the first depth at which the intensity started to decrease. This first point was determined as the point where: "the deviation was larger than two times of the standard deviation of the normalised intensity data within the flat region" [28]. In Figure 3.2a, a LAD can be determined of 0.6 mm, which is comparable to the LAD found in Figure 3.2b.

## Discussion and conclusion

Comparing the results from the simulation in Figure 3.2a to the results of Li et al. (2014) in Figure 3.2b, no discrepancies can be found. The intensity decreases around 4.4 mm noticeably for both curves and stops when the boundary reaches 5 mm. This results in a similar LAD of 0.6 mm for both simulations. Therefore, it is concluded that the simulation software has been configured accordingly.

## 3.3. Simulations parameters

### Materials

Compared to the test simulation, for the actual simulations cancellous and cortical bone were simulated by specifying their respective material properties. The wavelength of the simulated photons influences the absorption and scattering properties of the medium they travel through. In other words, the optical properties of the surrounding tissues change depending on the wavelength of the photons. Therefore, the tissue properties scattering coefficient, $\mu_s$, and absorption coefficient, $\mu_a$, were experimentally obtained from human cancellous and cortical bone and used as input for these wavelength-dependent parameters [3]. The experimental data were collected using a 1.2 mm core-to-core distance probe. The optical properties that remained constant during the simulation were the index of refraction (n = 1.44) and the mean cosine of the scattering angle (anisotropy factor g = 0.9).

### Light

Compared to the previous simulation, the amount of simulated photons was increased to obtain a better accuracy for the collected data. The number of photons for each simulation was set at 1e7. This amount of photons gives the best trade-off between simulation time versus the precision of the results. In Table 3.2, these simulation parameter can be found. The wavelength of the light that is simulated needs to be defined as well. As all measurements in this thesis are performed on optical bone phantoms, the addition of real blood is complex due to the lack of oxygen and sustenance in the bone phantom. Therefore, blood was not mixed into the bone phantom. As blood can be found throughout the bone, the lack of blood needs to be compensated. Looking at the optical properties of blood, it absorbs a large part of visible light [40]. As the visible part of the electromagnetic spectrum would have been absorbed by the blood, it is actually not used for detection purposes. Therefore, the decision was made to use light in the near-infrared range (NIR) between 1000 and 1600 nm for the experiments. For comparison, light in the NIR was also used during the simulations. As the presence of fat is used to detect the boundary between the cancellous and cortical layer, especially light with a wavelength of 1200 nm will be of interest. Thus, this single wavelength was used during the simulations. This had the advantage of significantly decreasing the simulations time.

The optical fibre used in the eventual prototype has a diameter of 200 microns. Therefore, this value is used in the simulations as well. A pencil beam was chosen as the beam type for the emitter. Although this type of beam is not the most representative type for emitted light from an optical fibre, this beam type is the most convenient to simulate.

### Simulation volume

The volume in which the photons are simulated needs to be specified. The dimensions of the cuboid space that need to be set are the width, depth and height. For both the width and length, 10 mm is used. The height of the cube is set at 7 mm. This dimension is used as the resulting volume allows the photons enough room to scatter while staying inside the simulation volume. Increasing the simulation volume adds more simulation time, while decreasing the volume results in photons getting lost as they leave the simulation volume and, thus, information is lost. The emitter and collector are placed on the y-axis at half the core-to-core distance

Table 3.2: The simulation parameters used in both the look-ahead distance and fibre configuration simulation.

| **Parameters used for both simulations** | |
|---|---|
| *Amount of photons* | 1e7 photons |
| *Wavelength light* | Wavelength: 1200 nm |
| *Emitter properties* | Pencil beam |
| *Collector diameter* | 200 microns |
| *Material properties* | Scattering ($\mu_s$) and absorption ($\mu_a$) coefficient are wavelength dependent, thus experimental data is used. Index of refraction (n): 1.44. Rutherford coefficient(g): 0.9. |
| *Simulation volume* | 10 mm x 10 mm x 7 mm (w x d x h). |
| *Bins* | x-direction: 201.<br>y-direction: 201.<br>z-direction: 500. |

from the centre.

The inside of the simulation volume is divided into so-called bins. The local information is stored inside these bins for later processing. The number of bins for both the x and y-axis was set at 201. This results in a resolution of 50 microns on both axes, which is deemed sufficient. The odd number of bins is chosen to prevent the emitter from being placed on the boundary between bins. The number of bins along the z-axis was set at 500. The number of bins was increased to obtain a better resolution along the z-axis as this is the direction of interest.

## 3.4. Look-ahead distance in cancellous bone

### Goal of simulation

The first simulation investigates the change in LAD for core-to-core distances larger or equal to 1.0 mm. This scenario is investigated as a larger LAD would give the instrument's user more time to react, and potentially, it could prevent the perforation of the cortical wall. The test simulation verified that the software was configured correctly as our simulation gave comparable results to the target study. This simulation aims to gain insight and obtain the LAD distance of optical fibres with a core-to-core distance between 1 and 5 mm in cancellous bone.

### Hypothesis

The LAD probably does not scale linearly, as the difference in LAD reported by Li et al. (2014) and Duperron et al. (2019) show [26], [28]. The most reasonable assumption is that the LAD increases along with the increase in core-to-core distance. It is hypothesised that the LADs will be between 0.5 to 1.5 times their respective core-to-core distances based on previously found LADs [26], [28].

### Method

The same method proposed by Li et al. (2014) is used for the first simulation. The parameters used for the simulation can be found in Table 3.2. A visual representation of the simulation volume can be found in Figure 3.1. The simulated core-to-core distance is 1 mm to 4 mm in steps of 1 mm. These distances were chosen as they would provide an overall indication of the change of LAD with regard to the change in core-to-core distance.

The core-to-core distances were increased to investigate the look-ahead distance in cancellous bone scales. A larger LAD is preferable as this allows the device's user to adjust the direction of the drill earlier based on the directional feedback. Although a larger LAD is expected for the increased core-to-core distances, the step sizes for the measurement depths were not adjusted. Based on the hypothesis, it was assumed this was not necessary.

The data from the simulations were analysed using Matlab. The data consisted of the detected number of photons found for each simulated distance to the cortical layer. The photons that reached the collector in the simulation can be interpreted as reflectance data as they were not absorbed in the subsequent layers.

The results were filtered using a moving average with a window of five. This was done as the intensities tended to have a larger deviation between simulated heights as the core-to-core distance was increased. Therefore, filtering made the curves more consistent and therefore, it was more convenient to obtain the LAD from the figure. After filtering, the data were scaled to the first simulation point, which only measured cancellous bone.

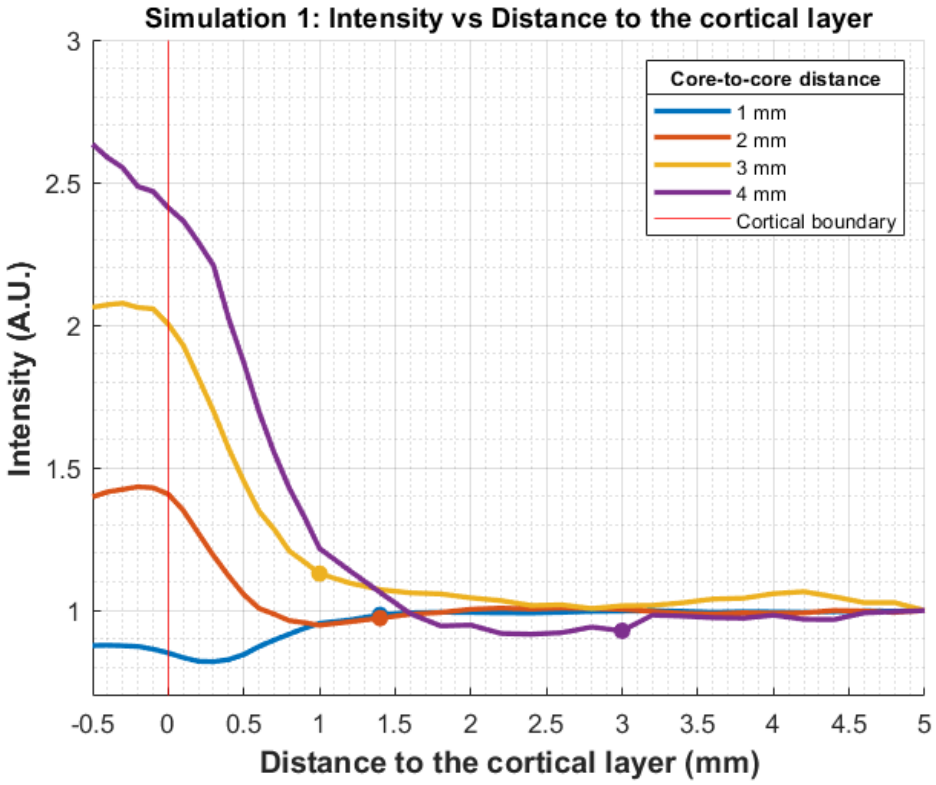


Figure 3.3: The intensity of the collected light with respect to the distance from the cortical is shown.

## Results

The resulting intensities that were derived from the first simulation can be seen in Figure 3.3. Coloured markers were used to indicate the first time the cortical layer is detected. The marker corresponds to the LAD for each of the different core-to-core distances. A marker is placed on the first measurement point where the difference between the average and the measured intensity is four times the standard deviation. The mean and standard deviation were calculated from the first ten data points starting from the top surface of the cancellous layer. The LADs for all the measurements are shown in Table 3.3. The last column from Table 3.3 contains the LAD over core-to-core distance.

## Discussion and conclusion

The goal of the simulation was to investigate how the LAD changes as the core-to-core distance are increased. The measured LADs align with the hypothesis that the LAD is 0.5 to 1.5 times the core-to-core distance except for the core-to-core distance of 3 mm. The LAD for the 3 mm core-to-core distance simulation is lower than expected. Looking at the yellow curve in Figure 3.3, this could be attributed to the small increase in intensity between 3.5 and 5 mm. This results in a higher standard deviation, resulting in a higher value that needs to be crossed for the LAD extraction. By simulating more photons, the deviation between the intensities decreases which could help in obtaining better estimations of the LAD.

Overall, the cortical boundary is detected earlier as an increasing core-to-core distance increases the LAD. This can be concluded from the data in Table 3.3, which contains the results extracted from Figure 3.3. Look-

Table 3.3: This table contains the LADs from the simulation results in Figure 3.3.

| Core-to-core distance (C2C) | Look Ahead Distance (LAD) | LAD/C2C |
|---|---|---|
| 1.0 mm | 1.4 mm | 1.4 |
| 2.0 mm | 1.4 mm | 0.8 |
| 3.0 mm | 1.0 mm | 0.33 |
| 4.0 mm | 3.0 mm | 0.75 |

ing at the ratio of LAD over core-to-core distance in Table 3.3, the increase in LAD seems to have a limit when increasing the core-to-core distance. By increasing the core-to-core distance, the volume through which the photons have to travel to reach the collecting fibre increases. This means that there are more changes for scattering events and absorption events to take place. These events become more dominant as the core-to-core distance is increased, thus limiting the increase in LAD. This phenomenon should be noted when increasing the core-to-core distance even further. However, the core-to-core distances are sufficient for this simulation, and an absolute increase in LAD was found. Therefore, these results show that the LAD increases when a large core-to-core distance is used.

An increase in intensity was expected as the distance to the cortical layer decreased. Fewer photons are absorbed by fat in the cancellous layer, leading to an increase in detected photons, and thus, an increase in intensity should be seen. This can be observed for the 2 mm to 4 mm core-to-core distances. The intensity for the core-to-core distance of 1 mm is not in line with the phenomenon mentioned above.

The decrease in intensity for the core-to-core distance of 1 mm was not expected. It means that for this core-to-core distance, fewer photons reach the collector as the cortical layer is approached. Besides the core-to-core distance, the amount of detected photons mainly depends on the absorption and scattering coefficient. The decrease in detected photons cannot be caused by absorption events as the amount of cancellous bone between the emitter and cortical layer decreases. This means there is less fat between the emitter and collector, and thus fewer photons are absorbed.

The scattering coefficient of cancellous and cortical bone at 1200 nm are $19.78cm^{-1}$ and $12.45cm^{-1}$ respectively. This decrease in the scattering coefficient as photons enter the cortical layer causes fewer scattering events to take place; thus, photons have less opportunities to make a "turn" towards the collector. Therefore, more photons cannot reach the collector for a core-to-core distance of 1 mm. For larger core-to-core distances, this decrease in scattering events has less influence. The path between the emitter and collector is longer; thus, more scattering events can occur for the photons to reach the collector.

In conclusion, by increasing the core-to-core distance above 1 mm, an overall increase in LAD is accomplished. It should be noted that for an increase in core-to-core distance, the diameter of the device needs to be enlarged to accommodate the core-to-core distance of the optic fibres.

## 3.5. Validating simulation results

### Goal of experiment

The results that were obtained from the simulations showed that by varying the core-to-core distance, a different LAD can be created. However, these simulations cannot perfectly replicate the real world. Therefore, the simulated results should be validated to see how relevant the simulated data is. This is done by experimentally obtaining DRS data that can be compared to the simulated results.

The goal of the experiment was to obtain the reflectance spectra of light on different depths inside a two-layered bone phantom using a multi-fibre probe. The spectra were collected using multiple core-to-core distances, similar to the core-to-core distances used in the simulations. By using the same core-to-core distance as were used during the simulations, a comparison can be made with the simulation results.

### Hypothesis

The results should show a comparable increase in intensity when the cortical layer is approached, as can be seen in Figure 3.3. However, a difference between a simulation and experimental setting exists. Compared to the simulations, a lot more photons are emitted during the experiment. This should make the results more accurate than those obtained by the simulations.

### Method

### Bone phantom

For the experiment, a bone phantom was made to imitate bone. The LAD is based on the amount of absorption of light by the fat inside the bone. Since the mechanical properties of bone are not necessary, a bone phantom was used that replicates the optical properties of real bone. The bone phantom consisted of two layers, the top layer replicated cancellous bone while the bottom layer resembled cortical bone. The cancellous bone was used as top layer as this is the bone type in which will be drilled during a procedure and because the cortical layer needs to be detected. The fat content of cancellous bone was replicated using coconut milk with a fat content of 17% which was added on top of the cortical layer when the experiment commenced.

The cortical layer was made using the ingredients listed in Table 3.4. The preparation of the cortical layer was done according to the following steps. First, distilled water was heated on a hot plate stirrer to 50 °C. Barium sulfate as added as scattering agent, sodium benzoate as a preservative agent and the NaCl to add ions to the distilled water. At 50 °C the gelatin was added and dissolved. The gelatin acts as a gelling agent and solidifies as the mixture cools down. The phantom was stored in the refrigerator till use.

Table 3.4: Materials used in the bone phantom production.

| *Layer* | Cancellous | Cortical |
|---|---|---|
| *Fat* | coco. milk, 17% | 0 ml |
| *Distilled water* | 0 ml | 100 ml |
| *NaCl* | 0 g | 1 g |
| *Sodium Benzoate* | 0 g | 0.1 g |
| *Barium Sulfate* | 0 g | 3 g |
| *Gelatin* | 0 g | 15 g |

## Setup

The DRS measurements for the experiment were performed using a DRS console (Philips, Netherlands). The DRS console is used in combination with a multi-fibre probe (Philips, Netherlands). By combining certain pairs of fibres, core-to-core distances between 1 and 4 mm could be formed. For this experiment, the following core-to-core distances were used: 1, 2, 3 and 4 mm, which are equal to the distances used in the simulation. In Figure 3.4a, the tip of the probe is shown.

The probe was attached to a precision stage with an accuracy of 0.01 mm (Thorlabs Inc. USA). The probe, along with the stage, were placed vertically above a bone phantom. This allowed the probe to be moved vertically and to collect data at different heights inside the bone phantom. The setup can be seen in Figure 3.4b.

First, the bone phantom was taken out of the refrigerator, to let it warm up to room temperature. Next, the optic fibres were connected to the DRS console. The calibration consists of two internal calibrations and a final calibration using the probe. This last calibration needed to be done each time the core-to-core distance was changed. This calibration was always done in a dark room. The calibration was performed by placing spectralon beneath the probe. Spectralon is a fluoropolymer that is used for diffuse reflectance standards as it gives the highest diffuse reflectance of any known material over the UV to near infrared region of the electromagnetic spectrum [41]. Therefore, spectralon is ideal to use as a reference for the DRS measurements. To account for the increase in core-to-core distance during the calibration, the distance from the probe to the spectralon was increased. The distances were set at: 2.3 / 4.5 / 6.7 and 8.8 mm for the core-to-core distances of 1 / 2 / 3 and 4 mm respectively. This ensured that light that reflected of the spectralon was able to reach the collecting fibre. The height of the probe in mm was determined using the following equation:

(a)

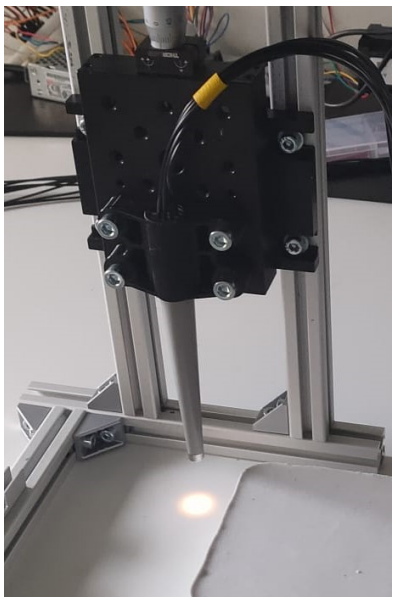

(b)

Figure 3.4: In (a), the setup used for the validation experiment is shown. The probe is mounted vertically. In (b), the head of the probe is shown. Each of the black dots represents a fibre tip.

$$z = \sqrt{(\frac{0.5x}{NA})^2 - (0.5x)^2} \tag{3.1}$$

Here x is the core-to-core distance in mm and NA the numerical aperture of the optical fibre, in this case 0.22.

After the calibrations, the tip of the probe was placed in contact with the bone phantom with the cancellous bone layer on top of the phantom. During each measurement ten samples are collected. After each measurement was done, the probe was lowered in steps of 0.2 mm from 50 to 10 mm above the cortical layer. For 10 mm to 0 mm above the cortical layer, steps of 0.1 mm were made to obtain a better indication of the LAD.

Unfortunately, the rigid bone phantom material in combination with the large frontal diameter of the probe caused the cancellous bone phantom to accumulate in front of the probe as the probe was pushed downwards. This meant that the probe always measured the accumulated cancellous bone. To mitigate this problem, the cancellous bone was first mechanically mixed to break up the rigid structure while maintaining identical optical properties. This did not solve the problem as accumulation of cancellous bone phantom still occurred. Therefore, a substitute was found in the form of coconut milk. Coconut milk has a fat content of 17%, which should result in a large enough fat concentration difference with the cortical layer. The lower viscosity of coconut milk compared to the cancellous bone phantom allowed the probe to move through the material unhindered and not accumulate in front of the probe. The experiment was done in reverse. The probe was positioned vertically and in contact with the cortical layer, after which coconut milk was poured onto the cortical layer. This prevented coconut milk getting trapped between the front of the probe and the cortical layer when the probe reached the boundary.

## Results

The DRS console obtains ten reflectance spectra per measurement point. The ten spectra were averaged, this made it easier to compare it to the reflectance spectra of the other measurement points. A centered moving average filter of five was used to compensate for outliers and to improve the consistency of the plotted curves. The resulting spectra were plotted in Figure 3.5.

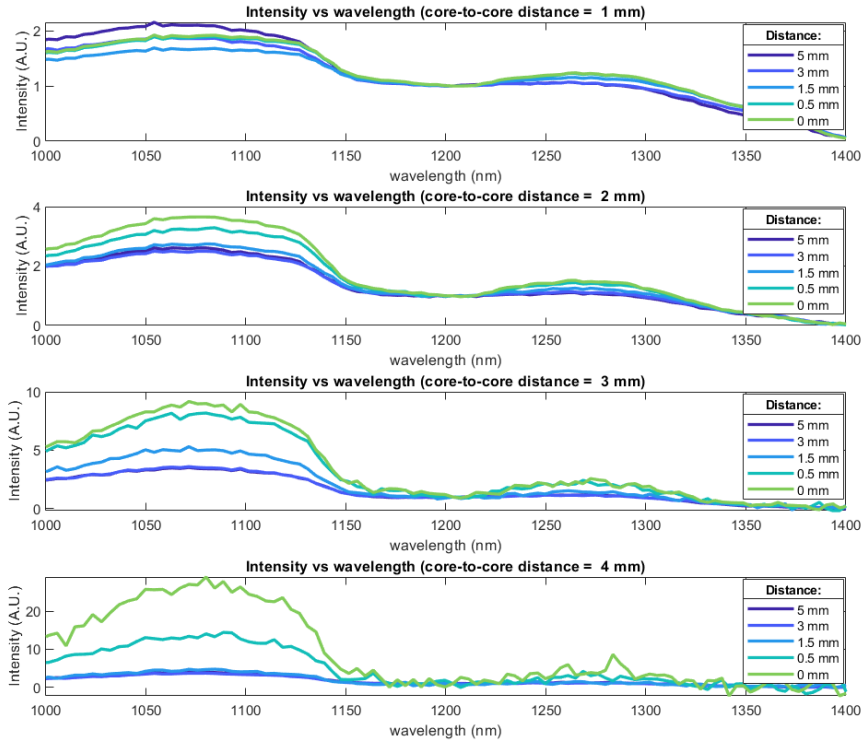


Figure 3.5: The reflectance spectra for different heights above the cortical layer are shown. Each graph was made using a different core-to-core distance.

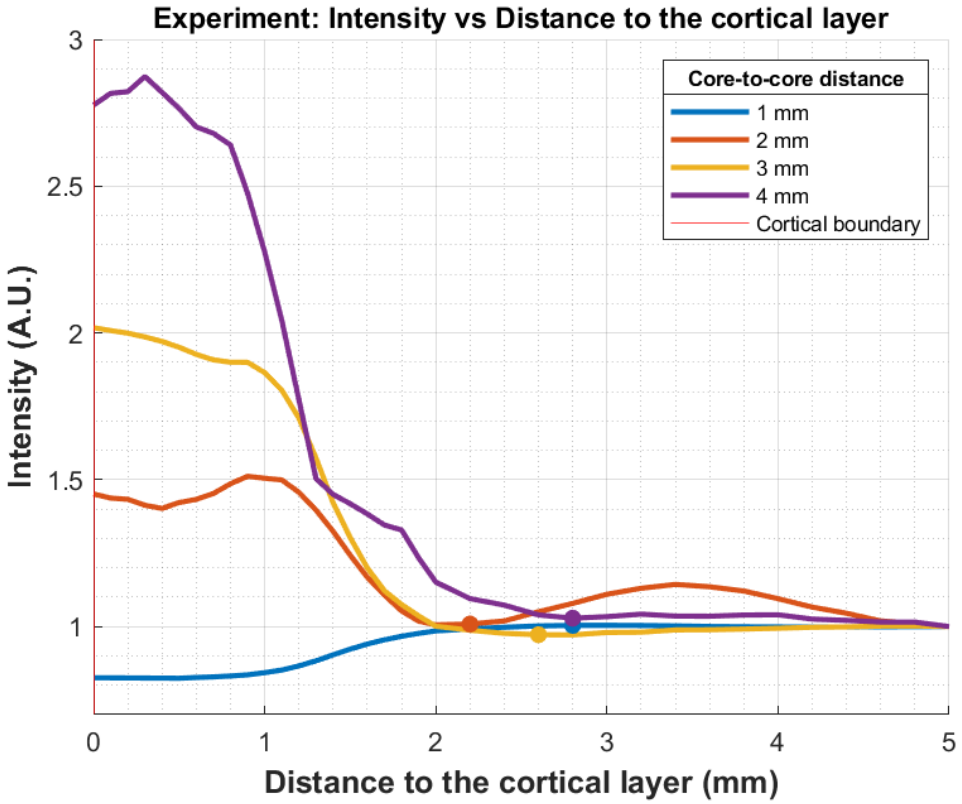


Figure 3.6: The measured intensity is plotted against shows the change of reflectance of the collected light with respect to the distance from the tip of the probe to the cortical layer.

Only a selection of the obtained spectra is shown to keep the curves distinguishable. The spectra were scaled to the intensity at a wavelength of 1200 nm as at this wavelength, fat absorbs light. This was done to provide a better indication of the differences between the different reflectance spectra.

Using the reflectance data from the wavelengths which light is absorbed by fat the LAD can be extracted. In Figure 3.6, the intensity of the reflected light around 1200 nm and plotted against the distance of the probe to the cortical layer. Colored markers indicate the point where the cortical layer is first detected. This way the LADs for each core-to-core distance can be clearly visualized. The markers also represent the LAD for each of the core-to-core distances. The markers are placed where the curve deviates from the mean by five times the standard deviation of the previous points. The mean was measured using the first ten data points in the cancellous bone. The amount of standard deviation was adjusted compared to the simulations to compensate for the higher amount of captured photons during the experiment compared to the simulations.

Using this method, the following LADs were identified for their respective core-to-core distance. The LAD are displayed in Table 3.5, along with the LADs found in the simulation.

Table 3.5: The results obtained from the experiment to validate the LADs obtained from the simulation. The experiment was done using four different core-to-core distances.

| **Core-to-core distance** | **LAD experiment** | **LAD simulations** |
|---|---|---|
| *1 mm* | 2.8 mm | 1.4 mm |
| *2 mm* | 2.2 mm | 1.4 mm |
| *3 mm* | 2.6 mm | 1.0 mm |
| *4 mm* | 2.8 mm | 3.0 mm |

### Discussion and conclusion

Comparing the LADs obtained from the experiment to the simulation results, a similar trend is found. In general, a larger LAD is observed for a larger core-to-core distance. Overall, the measured LADs are higher than the LADs obtained from the simulations. As more photons were emitted, a higher number of photons that travelled further ahead in the material can be collected again and thus influence the measured intensity. The increase in LAD in real life also means that the user can act on the feedback earlier if necessary. It should be noted that the LAD for a 1 mm core-to-core distance seems to deviate from the expected value (1.4 mm) by a large amount. Looking at Figure 3.6, a LAD of 1.8 mm would be expected. The difference can be caused by the calculation of the marker. Consistent measurements could cause the standard deviation to be low. A larger than normal deviation could have caused the marker to be placed at 2.8 mm.

Similar to the simulated 1 mm core-to-core distance, a decrease in intensity when the cortical layer is detected was also measured during the experiment. This strengthens the notion that this phenomenon is not an error but that the core-to-core distance has an influence on the change of intensity when the cortical layer is detected. The decrease in intensity should not be a problem for detecting a cortical wall. A change in intensity is clearly measurable, which is enough as a threshold to detect the cortical layer.

Based on the increasing intensity for a core-to-core distance of 2 mm and a decreasing intensity for 1 mm, there exists a transition between 1 and 2 mm where the change of intensity switches as the cortical layer is detected. If a core-to-core distance between 1 and 2 mm would be chosen, it should be a point of attention when testing the prototype.

During the experiment, the tip of the probe needed to be placed against the cortical layer. This introduced some inaccuracy as the cortical layer was flexible and the contact needed to be sufficient to keep coconut milk away from the tip during the first measurement. Therefore, to ensure no coconut milk flowed between the probe and cortical layer, the probe needed to be pushed slightly into the cortical layer. However, determining the exact depth needed was not possible. Therefore, an approach was used whereby the probe's tip was slightly pushed into the phantom. If the phantom could not be moved after contact, the probe placement was deemed correct.

Looking at the resulting LADs for the experiment, a core-to-core distance of 1 or 2 mm would be sufficient for the sideways LAD requirement. For the frontal LAD, a core-to-core distance of 2 mm could possibly be used. To ensure the requirement for a minimum LAD of 2 mm is met, a distance of 3 or 4 mm would be better.

From the experiment, two conclusions can be drawn. First of all, the frontal diameter of the probe used in the experiment was too large, which resulted in a buildup of material in front of the device. Therefore, this should be taken into consideration in the design phase of this thesis. The instrument needs to have a pointed/sharp tip that can push the cancellous bone to the side, thus preventing it from pushing a mass of material forward. This is in agreement with the requirement that the device should have a pointed tip for drilling.

Secondly, a distance of 3 mm would also be sufficient to meet the requirement without taken any inaccuracies into account. However, 4 mm provides the largest LAD whilst meeting the requirements. Therefore, this core-to-core distance will be used for a prototype. For the sideways sensing fibres a core-to-core distance of 1.5 mm was chosen as it is expected that this will meet the required 1 mm LAD.

## 3.6. Simulating fibre configurations

To obtain directional feedback from within the pedicle, it is necessary to have at least one fibre that collects light at a different angle from the frontal fibres. This allows the emitted light to be collected from at least two different directions, and thus, information is obtained from the tissue volume surrounding the drill. In turn, this information can be turned into feedback on the orientation of the drill inside the pedicle.

For sensing in the pedicle, two directions were deemed essential. The first direction is along the central axis of the drill and this will be referred to as the axial direction. The axial direction is necessary to detect the cortical layer at the other side of the bone body. The second direction is in the direction perpendicular to the drill and will be referred to as the transverse direction. Sensing in transverse direction allows the pedicle wall surrounding the drill to be detected. With this in mind, two general fibre designs were made that can be implemented into an instrument to test for directional feedback:

- ***Design 1:***
  The first design has one collecting and one emitting fibre at the front in combination with one collecting fibre at the side. The emitting fibre at the front of the instrument provides light for both collecting fibres. Both collecting fibres are sampled at the same time. Therefore, opposed to the previous design,

attention should be paid to the signal-to-noise ratio of both collectors, which will mainly depend on the core-to-core distances used. For Design 1, the light needs to make a 270° turn to reach the sideways facing fibre. Consequently, the longer path to the collector results in a lower signal-to-noise compared to a similar core-to-core distance for a frontal fibre pair. If the signal-to-noise ratio of the collected light is too low, the accuracy of the sideways data is impaired. Therefore, it is essential to find the right configuration for the sideways fibre for which the signal-to-noise ratio is viable to be used and comparable to the frontal collector. This design can be found in Figure 3.7a.

- ***Design 2:***
  The second design has one collecting and one emitting fibre at the front in combination with one collector and one emitting fibre at the side. This configuration of the fibres allows the pairs to be individually used. In case the fibres are used simultaneously, the light emitted by both pairs must not interfere with each other. In other words, the frontal collector fibre should not collect the light emitted by the non-paired fibre as this would introduce noise into the collected signal. A solution is to sample the pairs in succession. However, this means a decrease in information as the sample rate is halved, which is not preferable. The signal-to-noise ratio can be increased by placing the pairs far enough apart so each pair receives little to no light from the other pair. In Figure 3.7b, this design is illustrated.

It should be noted that these designs are the most basic fibre configurations that can be made. Other designs using more fibres are a possibility. However, more intricate designs with a higher number of fibres are harder to simulate and produce, and will not necessarily add any value. It should be noted that the possibility exists that more fibres could provide better feedback however, the proposed designs are sufficient for obtaining the data that is needed to make a decision on the fibre configuration as well as testing of a prototype.

In Figure 3.7, both designs are schematically visualised. The green lines represent the emitting fibres, while the red lines represent the collecting fibres. The yellow lines show a possible path that the photons can take to reach the collecting fibre.

## Goal of simulation

The designs that were previously described have their advantages and disadvantages. Design 1 needs fewer fibres, leading to a more compact design; however, the sideways facing fibre could possibly have a lower signal-to-noise ratio compared to the forwards facing fibres. Design 2 will lead to a longer instrument as the fibre pairs should not interfere however, this design is able to sense in different directions independently. This simulation is done to compare both designs and to find the most suitable one for a prototype. The different configurations of both designs are compared by changing the distance between the emitting and collecting fibres.

A ratio is calculated by dividing the number of photons that reaches the sideways collector by the number of photons that reaches the frontal collector, as is shown in Equation 3.4. This is used to determine if the collecting fibres in Design 1 collect a similar amount of light thus have a similar signal-to-noise ratio. Such a configuration would inherently be unsuitable for Design 2. This principle can be applied vice versa for ratios indicating large disparity in the amount of collected photons.

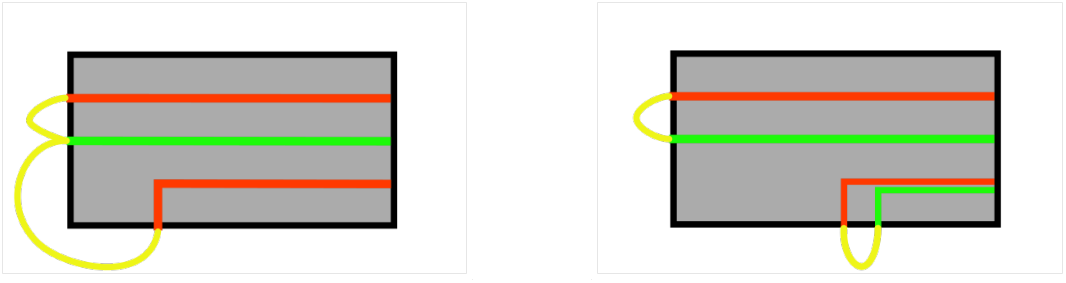

(a) *Design 1* (b) *Design 2*

Figure 3.7: Both fibre designs that could be implemented in a prototype are illustrated. Design 1 has two collecting fibres and a shared emitting fibre. Design 2 contains 2 fibre pairs for individual sensing in both directions. In both designs, green represents the emitting fibre(s), red the collecting fibres and yellow a possible path for photons.

## Hypothesis

An increase in the distance between the emitter and collector leads to an overall decrease in collected photons. In addition, the distance that photons need to travel to reach the sideways collecting fibre for Design 1 is longer than the path between the front fibres. Therefore, the forward facing fibres will collect more photons and thus overall more configurations will be found that have ratios above one. Ratios of one are likely to be found for configurations where the distance between the sideways facing fibre and frontal emitter is small.

## Method

In Figure 3.8, the simulated configuration can be seen. Design 1 was simulated as for this design the fibre configuration matters most. This is the case as both collecting fibre need to have a similar signal-noise ratio. The configurations that are not deemed suitable for Design 1 are inherently suitable to be used in the second design as for this design the fibre pairs should not interfere. The simulation was divided into two parts as only one collector can be implemented per simulation.

In the first part of the simulation, the emitter and the sideways facing collector were simulated to obtain the number of detected photons on the sideways collector. This was done for configuration with a $d_s$ between 1 mm and 5 mm with increments of 1 mm. In Figure 3.8, $d_s$ represents the side core-to-core distance.

The length of $d_s$ is an hypotenuse which legs consist of $d_l$ and $d_w$. During the simulation, the length of $d_w$ was kept constant, with its length being:

$$d_w = d_{wall} + \frac{d_{fibre}}{2} \tag{3.2}$$

Here, $d_{wall}$ represents an assumed wall thickness of 0.75 mm and $d_{fibre}$ a fibre thickness of 0.2 mm. The reason for keeping $d_w$ a constant value is that the wall thickness has to be kept to a minimum. Extra space between the fibre and wall adds no extra value and increases the diameter of the instrument. According to the requirements, the diameter cannot exceed a maximum distance of 6 mm.

To obtain the different configurations for $d_s$, the $d_l$ was varied by using the values of $d_s$ as input. The variable $d_l$ was calculated by:

$$d_l = \sqrt{d_s^2 - d_w^2} \tag{3.3}$$

For the second part of the simulation, the emitter and the frontal collector were simulated while the $d_f$ was step wise increased. The values for $d_f$ were kept the same as $d_s$ to facilitate the comparison of the results.

For both simulations, the volume only contained cancellous bone. Cortical bone was omitted as no boundary detection is needed for this simulation and the primary material that is drilled during spinal surgery is cancellous bone. The other parameters were kept the same as reported in Table 3.2.

The amounts of detected photons for the different configurations of $d_f$ and $d_s$ that were used to calculate the ratio between the signal obtained from the frontal collecting fibre compared to the signal from the sideways collecting fibre. The ratios were calculated using the following equation:

$$r = \frac{n^{d_s}}{n^{d_f}} \tag{3.4}$$

Here $n^{d_s}$ and $n^{d_f}$ stand for the amount of detected photons for $d_s$ and $d_f$ respectively. Using the ratios, the different fibre configurations were compared to see which configuration are suitable for Design 1.

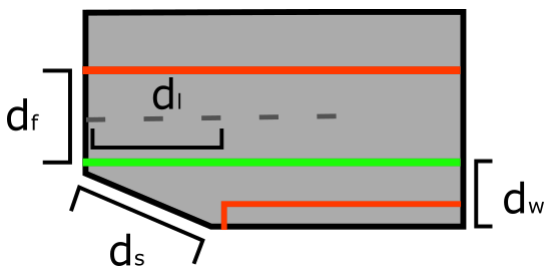


Figure 3.8: The geometry that was used for simulation. (The scale in both figures is not representative.)

Table 3.6: The table contains the ratios that were calculated in Simulation 2.

| | | $d_s$ | | | | |
|---|---|---|---|---|---|---|
| | | 1 mm | 2 mm | 3 mm | 4 mm | 5 mm |
| $d_f$ | 1 mm | 0,01 | 0,05 | 0,28 | 1,04 | 2,43 |
| | 2 mm | 0 | 0 | 0 | 0 | 0 |
| | 3 mm | 0 | 0 | 0 | 0,01 | 0,02 |
| | 4 mm | 0 | 0 | 0 | 0 | 0 |
| | 5 mm | 0 | 0 | 0 | 0 | 0 |

## Results

The resulting ratios are shown in Table 3.6. The table contains the ratios of collected photons for each of the simulated configurations (Figure 3.8). The rows corresponds to the core-to-core distance of the frontal fibres, $d_f$. The columns correspond to the core-to-core distance from frontal emitter to the side collector, $d_s$.

Colour was used to indicate the viability of the corresponding configuration in Table 3.6. Red indicates ratios between 0 and 0.4 or above 2.5. These ratios indicate that the configuration is not viable for use as the disparity between the number of photons collected on the front and side is too large and not usable. Orange indicates ratios between 0.4 to 0.8 and 1.2 to 2.5. These ratios can be used for both design, however this is not preferable. Green indicates ratios between 0.8 and 1.2. These ratios indicate that the configuration can be used as a comparable number of photons reaches both detectors.

As can be seen in Table 3.6, most of the ratios are close to zero. The low ratios indicate that the number of photons detected by the sideways collector is minimal. For a $d_f$ of 1 mm, and a $d_s$ of 4 mm and higher, the ratio was close to one.

## Discussion and conclusion

The calculated ratios indicate which configurations are suitable for which design. For Design 2, both the collectors receive light from the same emitter. To obtain a similar accuracy for both collectors, the signal-to-noise ratio needs also be similar as well. Therefore, ratios close to one are configurations that can best be used for Design 2. However, the ratios in Table 3.6 indicate that minimal to no light reaches the sideways collector. The only configurations that could be used need to have a frontal core-to-core distance of 1 mm. However, the simulations indicate that this would be insufficient to obtain the wanted LAD of 2 mm.

In Design 2, obtaining a similar signal for both fibres mainly depends on the signal that reaches the sideways facing collector. To reach this collector, light needs to traverse a longer path because of the 270°turn it needs to make. This probably caused less light to be collected by the sideways facing collector and thus the ratios are close to zero were obtained.

The results in Table 3.6 show that Design 1 is the most suitable as the majority of the configurations have ratios close to zero, indicating that far less light reaches the location of the sideways facing fibre. By placing a sideways looking fibre pair in this location, less to no noise is received from the frontal fibre pair.

The goal of the simulation was to see which design could be best implemented for a prototype. Based on the results, it can be concluded that the majority of the configurations were suitable for Design 2. In addition, the configurations suitable for Design 1 would not be able to produce the required forwards LAD. Therefore, the decision is made to use the fibre configuration from Design 2, with two optical fibres on the front of the device and two optical fibres at the side of the device.

# 4

# Design of prototype

## 4.1. Requirements for the prototype

After the simulations, the following conclusions were made. First, it was concluded that the prototype would have two frontal and two sideways looking fibres (Design 2, Figure 3.7b). Secondly, according to the validation experiment, a core-to-core distance of 4 mm was necessary to obtain the minimally required LAD of 2 mm. These design parameters will be taken into account in the design of the prototype.

Generally, the prototype consists of three separate parts, which can be seen in Figure 4.1. Part A, in light blue, is responsible for securing the tubing running through the prototype as these tubes contain the actual optic fibres. Part B, in red, is responsible for holding the tubing in place inside the device. In addition, Part B guides the tubing and fibres to their respective positions where the fibres will need to enter Part C. Lastly, in yellow, Part C represents the tip of the device that holds the fibre ends, and this is the Part where the light is emitted and collected. Part C also penetrates the bone, and therefore, the tip should have a pointed end which helps with easier penetration and prevent material from building up in front of the device.

A modular build-up makes the insides of the prototype more accessible, and thus it makes the prototype easier to assemble. Therefore, the prototype's build-up, as shown in Figure 4.1, was chosen. It should be noted that the prototype that is proposed in Figure 4.1 is a general form for the prototype, and this sketch should not be considered a final design for the prototype.

In Chapter 2, the requirements that the eventual prototype needs to adhere to, were already discussed. These design requirements will used to test the prototype. Thus, by looking at those criteria, several points were identified that have to be considered during the design process. These points are the following: strain relief, fibre containment inside the body, sensing sideways to the drill direction, sensing forward, and the protection for the fibre tips. For the overall design, these points were used in the concept generation for the device.

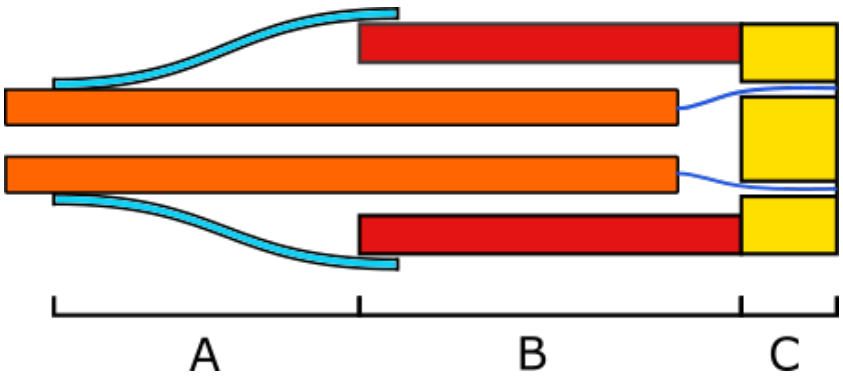


Figure 4.1: The general build-up for the proposed prototype. It consists of a strain relief for fibre tubing (A), a body to guide and secure the fibre tubing (B) and the tip of the device (C) which is responsible for sensing.

## 4.2. Solution Generation

***Part A***

To generate different concepts for the prototype, a morphological chart is made using each of the points mentioned as shown in Table 4.1. Each of the rows in the morphological chart corresponds to a previously described solution. Each column contains a solution for each corresponding point, which can be used to create a concept.

Part A mainly acts as a strain relief for the tubing containing the optic fibres. The outer tubing needs to be connected to the DRS console in order for the light to reach the device. This loose tubing can get stuck while being moved, resulting in an external force being applied to the tubing. This would result in either damaging or dislodging the fibres at their connection points inside the device, thereby affecting the device's usability. By integrating a strain relief system, these problems can be prevented.

***Part B***

The optic fibres used for the prototype are made by Thorlabs, Inc, (US). The fibres consist of an outer protective tubing (orange). Inside this tubing, the optic fibre is loosely contained. This allows for some space so the fibre can move inside the tubing and thus prevent stress from damaging the fibres. The actual fibre (blue) is coated again to prevent light from entering and escaping the fibre. The optic fibres are fragile by nature, and although they are encased in a protective coating and tubing, the fibres need to be handled with care. Besides Part A, Part B will also be used to secure the fibres inside the device's body properly. This will prevent the device's movements from dislodging the integrity of the fibres. In addition, the body can be used to hold and secure the device during the testing of the prototype.

***Part C***

The primary function of Part C is to house the optic fibres that are inserted into the body. However, multiple points need to be integrated into Part C. First of all, the solutions for mounting the forward sensing fibres in the tip of the device are discussed in Part C1. Secondly, for the sideways sensing fibres, a mechanism needs to be incorporated to ensure that light can be emitted and collected sideways at an angle of 90°. These solutions are explained in Part C2. Lastly, the tips of the fibres will need to be protected from wear and abrasion. These solutions are discussed in Part C3.

Table 4.1: The morphological chart of the proposed solutions for each part of the prototype.

| Section | Main goal | 1 | 2 | 3 | 4 | 5 |
|---|---|---|---|---|---|---|
| A | Strain relief | 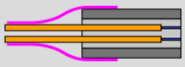 | 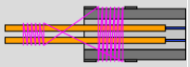 | 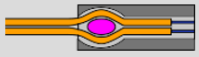 | 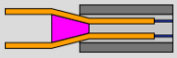 | 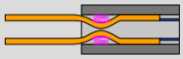 |
| B | Body | 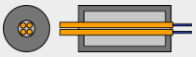 | 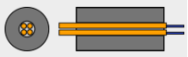 | 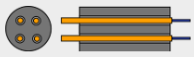 |  | |
| C1 | Forward Light Emission |  |  | | | |
| C2 | Sideway Light emission/ collection | 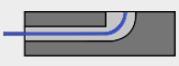 | 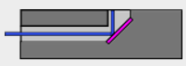 | 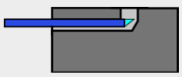 | | |
| C3 | Fibre tip protection |  | 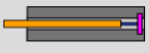 | | | |

### 4.2.1. Part A: Strain Relief

***Solution A1***

For Solution A1 (Figure 4.2), a stiff sleeve acts as strain relief around the fibre tubing. The sleeve presses the fibre tubes together and stays in place due to friction. The other end of the sleeve is pulled over the device's body. Forces acting on the tubing are transferred to the sleeve, which absorbs the forces by elastic deformation. An advantage is that the stiffness of the sleeve also prevents the fibre tubes from bending beyond their minimum allowed radius.

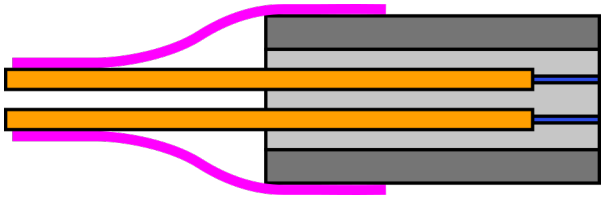

Figure 4.2: Solution A1

***Solution A2***

For Solution A2 (Figure 4.3), metallic wires are wound around the fibre tubes and the body. This solution is similar to the Solution A1 but is more flexible in its application. The advantage is that the number of windings can be easily adjusted. By increasing the number of windings around the fibre tubes, the chance of slipping when an external force is applied to the fibre tubes can be reduced. The same goes for the windings around the body, although slippage on the body can be prevented using a slot where the windings can be placed. A point that would require attention is that the windings should not cut into the body of the fibre tubes.

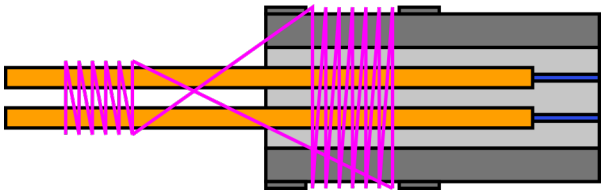

Figure 4.3: Solution A2

***Solution A3***

For Solution A3 (Figure 4.4), the inside of the device's body has multiple curves in which the fibre tubes are laid. This principle can be compared to coiling a rope around a drum, in which the force is necessary for the rope to be pulled. Therefore, external forces on the fibres tubes can be absorbed through friction. A disadvantage is that multiple curves are needed to obtain a sufficient increase in friction. However, the fibres have a minimum bending radius that cannot be crossed in order to avoid damages. This would result in an increase in the diameter and as well as the length of Part B, the body.

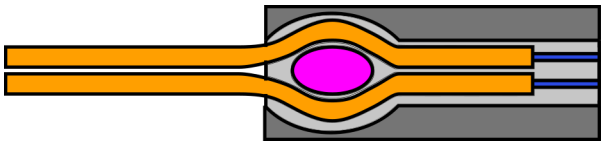

Figure 4.4: Solution A3

***Solution A4***

For Solution A4 (Figure 4.5), a wedge acts as a strain relief. The wedge can be applied in multiple ways. It could be applied and pre-loaded during assembly such that the wires stay in their assigned places. Another application would be to make the body such that the wedge can be inserted into the body. This way, the wedge will not prevent the fibres from being pushed into the body during assembly. However, when an external force is applied, thereby pulling the fibre tubing out of the body, the wedge will be pulled along, causing the fibres to become stuck.

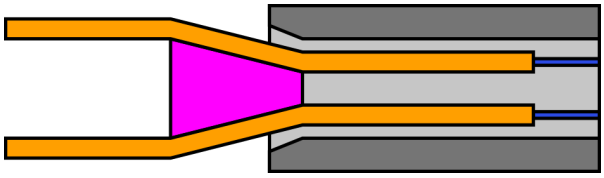

Figure 4.5: Solution A4

***Solution A5***

For Solution A5 (Figure 4.6), springs are used to create a clamp. The clamp will push down onto the tubes and act as a strain relief. The advantage of this solution is that the friction between the fibre tubes and clamp can be adjusted by selecting different springs. However, the assembly will become harder due to the increase in components and the compression that the springs will need during assembly.

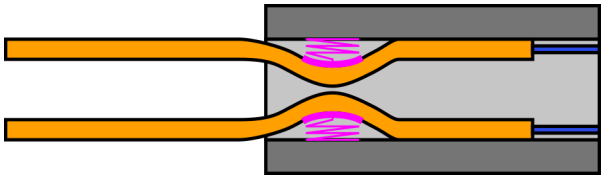

Figure 4.6: Solution A5

### 4.2.2. Part B: Body

***Solution B1***

For Solution B1 (Figure 4.7), the fibres enter the body together through a single hole, as shown in Figure 4.7. This hole is made as small as possible in order to provide friction on the tubes. Inside the body of the instrument, the fibres will be given space. This has the advantage that more fibre tubing can be stored inside the device. In case of an external force that is applied on the fibre tubing outside the device, the extra fibre tubing could straighten out before the force is exerted onto the fibre itself. The fibre tubing will again exit the body through a hole where the optic fibres will go into the device's tip. The extra space can also be used to incorporate some of the strain relief solutions.

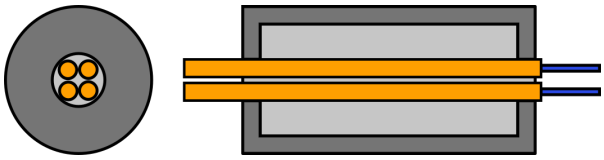

Figure 4.7: Solution B1

***Solution B2***

For Solution B2 (Figure 4.8), the fibre tubing is constrained along the whole length of the body, as shown in Figure 4.8. Similar to Solution B1, the four fibre tubes enter the body together. Besides keeping the diameter of the body smaller, this way of entry has the advantage that the optic fibres are closer to the centre of the body and thus require less bending of the fibres at the end of the body to enter the tip of the device. The tubes cannot move inside the body. By keeping the fit between the tubing and walls tight, the friction between the walls and tubes can be used to keep the tubes in place in case of an external force.

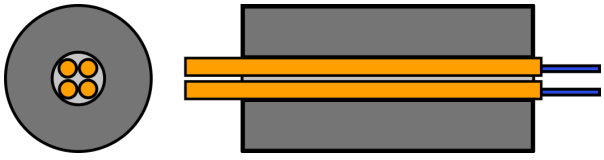

Figure 4.8: Solution B2

***Solution B3***

For solution B3 (Figure 4.9), the fibres are also constrained along the whole length of the body. However, in this case, each fibre is constrained separately, as illustrated in Figure 4.9. This is done to ease assembly. However, the diameter of the body becomes larger. This increase is not a concern as the body does not enter the bone, but the optic fibres lay further from the centre of the body and thus require more bending to enter the tip of the device, which is a point that should be paid attention to should this solution be incorporated into the prototype.

Figure 4.9: Solution B3

***Solution B4***

For solution B4 (Figure 4.10), the fibre tubing is exposed along the outside of the body. A lot less material is needed to make this body, and the fibres can be easily attached to the body. Each of the tubes has its own slot in which they are placed.

Figure 4.10: Solution B4

### 4.2.3. Part C: Tip

### Part C1: Forward sensing fibres mounting

The forward sensing fibres are the most straightforward to attach. The two optic fibres run from the body to the front of the tip. Here the fibre tips should have an unobstructed view in front of the tip. This way, they can emit light into the material in front of the device and collect it again. Two different solutions for a design were made and are explained below.

***Solution C1-1***

For Solution C1-1 (Figure 4.11a), the optic fibres run along the outside of the device, as illustrated in Figure 4.11a. A trade-off is made by lowering the amount of fibre protection and thus lowering the tip diameter as a result. The core-to-core distance has become the tip diameter. For this solution, to create some protection, the fibres could be coated with an additional layer of adhesive to form a protective coating for wear. The coating also helps to keep the fibres secured.

***Solution C1-2***

For Solution C1-2 (Figure 4.11b), the fibres are integrated into the tip and not left exposed, as shown in Figure 4.11b. The extra wall that is added between the fibre and the outside offers extra protection at the expense of the tip diameter. However, this extra layer of a wall can be minimized depending on the material that is used.

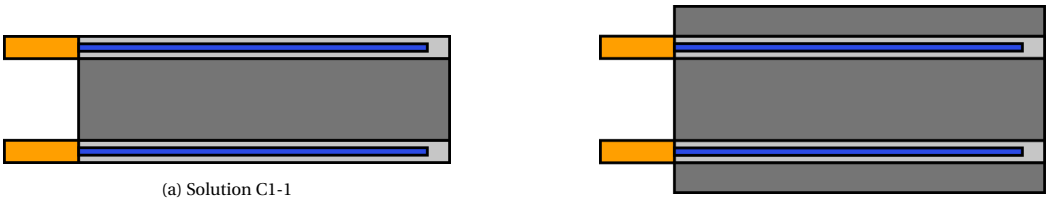

(a) Solution C1-1

(b) Solution C1-2

Figure 4.11: The solutions proposed for Part C1.

## Part C2: Emitting and collecting light sideways

***Solution C2-1***

For Solution C2-1 (Figure 4.12), the wire is bent such that it emits perpendicular to the surface of the device tip, as seen in Figure 4.12. This solution is the most straightforward method that can be used. By laying the fibre along a groove in the tip, the assembly would be easy. However, to make this solution work, the bending radius of the fibre needs to be determined. Looking at Table 2.1, the maximum bending radius that can be used is 12 mm in the short term and 24 mm in the long term. However, using either of the bending radii results in the diameter of the tip exceeding the maximum diameter of the tip set in the requirements. This means that this solution is not viable with the current optic fibres.

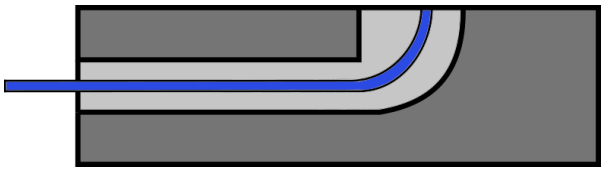

Figure 4.12: Solution C2-1

***Solution C2-2***

For Solution C2-2 (Figure 4.13), reflection is used to emit and collect the light at a 90° angle. At the location where the light needs to be emitted, a ramp at a 45° angle is placed. In Figure 4.13, the purple area indicates the reflective surface placed on a ramp. This reflective surface can be accomplished by either placing a piece of metal or applying a reflective coating. The advantage of this solution is that the fibre stays straight, and not much space is needed to sense in a sideways direction. This helps in keeping the diameter of the device tip minimal.

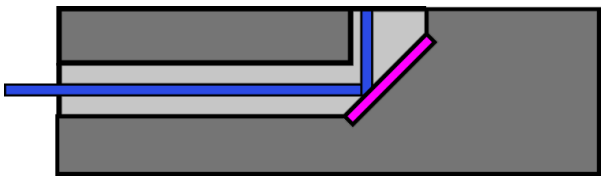

Figure 4.13: C2-2

***Solution C2-3***

For Solution C2-3 (Figure 4.14), the fibre tip is adjusted by slanting and removing a small part of the coating at the tip, as is shown in Figure 4.14. A patent by Yadlowsky et al. (2014) describes these modifications to a fibre tip to create a reflective surface [42]. They use the internal reflection of light on the slanted surface together with refraction, so the light leaves the fibre on the side. The light is then emitted perpendicular to the fibre.

Using the fibre as the tool to emit sideways has multiple advantages. The fibre can be incorporated in a straightforward fashion without any bending of the fibre. In addition, no additional parts are needed to reflect the light. This makes the design easier to produce. However, in order for this solution to work correctly, the tip needs to be slanted at the correct angle, which is relatively difficult for a fibre with a diameter of 0.2 mm. Besides the slanted tip itself, the fibre needs to be fixated in such a fashion that the light is refracted correctly into the surrounding material.

(a) (b)

Figure 4.14: In (a), Solution C2-3. In (b), a detailed view of the tip of the fibre. The dark blue coating is removed leaving the optical fibre exposed. The tip is slanted to create a reflective surface. The yellow line represents the light reflecting and refracting.

### Part C3: Fibre tip protection

At the tip of the device, the optical fibres emit and collect the light. This means that at the front and side of the device, the fibre tips need to have a clear line of sight to the surrounding bone. However, leaving the tips exposed to the bone whilst drilling is not a solution. Duperron et al.(2019) enhanced a drill by integrating optic fibres for DRS[26]. In their design, the fibre tips were left exposed at the cutting surface. They found that the tips were prone to abrasion and damage. To prevent the same from happening, the fibre tips will have to be covered or separated from the materials that are drilled into. A clear medium in the NIR range is necessary so light can still pass through unhindered.

***Solution C3-1***

For Solution C3-1 (Figure 4.15), the fibre tips are protected using a silica plate or disk that is placed in front of the fibre tips. This is also the solution proposed by Duperron et al. (2019). Besides certain types of silica being transparent in the near-infrared range [43], another advantage of silica is that the assembling would be simple as it only entails placing the silica. However, acquiring and producing the silica could be difficult.

Figure 4.15: Solution C3-1

***Solution C3-2***

For Solution C3-2 (Figure 4.16), an adhesive is used to secure the fibre tips. The adhesive can be applied after the assembly of the device. The adhesive behaves as a transparent plug at the end of the hole through which the light is emitted and collected, thereby keeping material out as well as protecting the fibre tips from abrasion. In addition, by placing the fibre tips near the end of the instrument's tip, the tip will also come into contact with the adhesive. This way, the fibre tips are held in their intended positions and are not able to move.

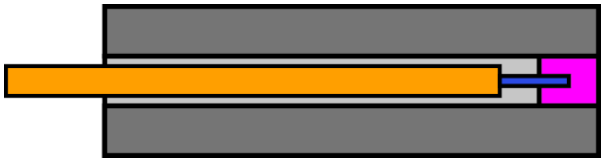

Figure 4.16: C3-2

Table 4.2: The morphological table containing the proposed solutions. The coloured lines (black,green and blue) under the solutions can be combined into the generated designs for the prototype. The diagonal red lines indicates the rejection of the corresponding solution.

| Section | Main goal | 1 | 2 | 3 | 4 | 5 |
|---|---|---|---|---|---|---|
| A | Strain relief | 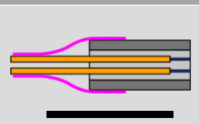 | 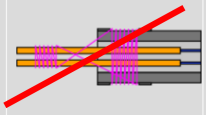 | 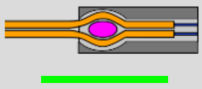 | 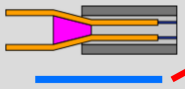 | 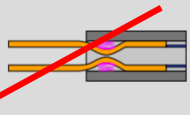 |
| B | Body | 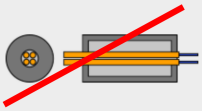 | 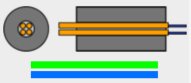 | 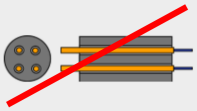 |  | |
| C1 | Forward Light Emission | 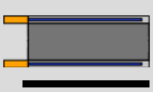 |  | | | |
| C2 | Sideway Light emission/ collection | 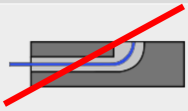 | 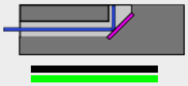 |  | | |
| C3 | Fibre tip protection |  | 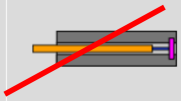 | | | |

## 4.3. Concepts generation

To generate different concepts for a prototype, the different solutions from each row in Table 4.1 are combined, which is visualized in Table 4.2. To reduce the number of possible concepts the solutions in each row were checked on their viability.

Solutions A2 and A5 were deemed to be unsuitable. The wire in Solution A2 could easily damage the fibre tubing. Solution A5 was rejected as the springs in the design would complicate the design unnecessarily.

Solutions B1 was rejected because the amount of internal space needed to make the solution suitable was deemed too large and therefore a waste of space. The individual containment of the fibre tubes in Solution B3 had no clear advantage over Solutions B2 and B4 while having a larger diameter. Therefore, this solution was also not taken into account during the concept generation. Lastly, the Solution of C3-2 which uses the silica cover to protect the fibre tip was not used during the concept generation. The advantages of Solution C3-1 outweighed the advantages of Solution C3-2 as the adhesive can be used to take care of the protection as well as the fixation of the fibres while being easier and more flexible to apply.

In Table 4.2, the morphological table that was used for the concept generation is shown. The discontinued solutions are indicated using a red diagonal line. By combining the solutions together, three concepts were generated. The solutions that combine into a concept are indicated using coloured lines (black, green and blue). The solutions for each concept were combined based on the synergy between the solutions. The three concepts were given scores to determine which concept would be the most suitable for creating a prototype. It should be noted that each of the concepts will have to be turned around their central axis to obtain data from their surroundings and thus, be able to provide 3D feedback.

***Concept 1: Minimalized cross-section***

The first concept is made from the solutions that are underlined with black in Table 4.1. The rubber sleeve that works as strain relief was chosen in combination with a body for which the fibre tubing runs along the outside of the body. This was done to enlarge the contact area between the rubber sleeve and the fibre tubes. An example of the sleeve and body can be seen in Figure 4.17. The sleeve covers the whole body (Part B) till it only contains the fibre tubes. The actual length that covers the fibre tubing is variable.

The frontal facing optic fibres run along a groove in the outside of the tip towards the front. As mentioned

earlier, this does leave the fibres exposed to the surrounding material. However, the front of the tip will have the most direct contact with the cancellous bone. This means that most of the abrasion and wear will happen here as well. Nevertheless, the coating around the fibre could still be damaged. By applying an adhesive along the entire exposed length of the fibre, wear can be prevented. The advantage of this placement of the fibre tubing and fibres is that the diameter of the tip can be kept to a minimum which would be 4 mm as the diameter of the device would be equal to the required core-to-core distance of the frontal fibres. An additional layer of adhesive will not result in a large increase in the diameter.

The optic fibres that are used for the sideways light emission and collection run through the middle of the tip, as can be seen in Figure 4.17. The core-to-core distance for the sideways sensing fibres is 1.5 mm and therefore smaller than the core-to-core distance of the frontal sensing fibres. In this case, the sideways sensing fibres can be placed in between the forward sensing fibres. This helps to reduce the frontal area of the tip which makes drilling easier.

To emit the light perpendicular to the side of the tip, a reflective surface is placed in front of the sideways sensing fibres, at a 45° angle. This allows the light to shine at 90° in a transverse direction. In a similar fashion, the light is collected again. To prevent light from directly entering the collecting fibre as soon as it is emitted, a wall is placed in between the two fibres. This wall extents to the reflective ramp. This way the light has to enter the surrounding material in order to reach the collecting fibre.

The fibre tips are protected using a clear adhesive. As mentioned before, this will also help keep the fibre tip in the correct position. This method was chosen as the fibres will run along the outside of the tip. Therefore, there is no wall in which a piece of silica could be mounted. In addition, as adhesive is already applied in this concept this would be more convenient during the assembly of the device.

One of the disadvantages of the current concept is that adjusting the prototype would be problematic as the adhesive will coat a portion of the fibre. Therefore, the tip and part of the fibre cannot be reused should the prototype need to be dismantled.

On the other hand, the fact that the fibres will run along the outside of the tip means that the tip's internal structure can be solid. This will make the production of the tip easier as well as more resistant to bending.

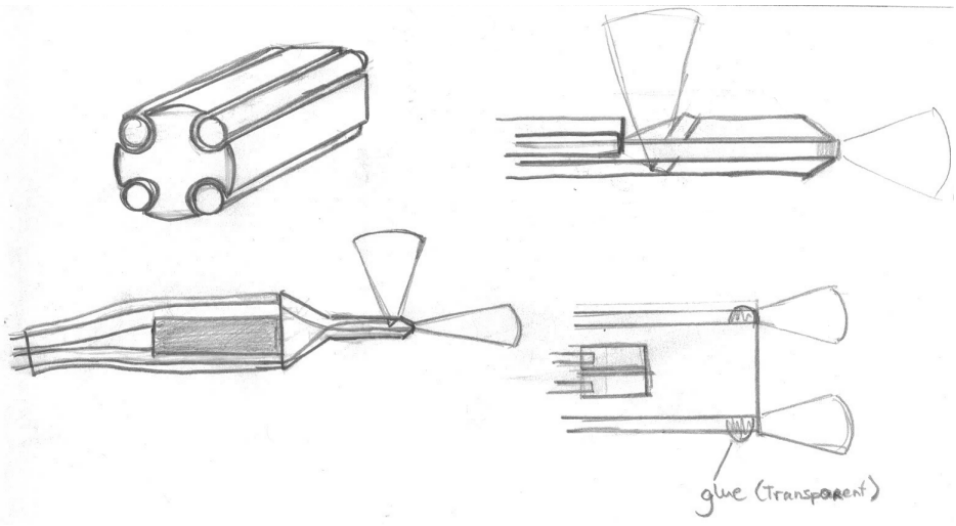


Figure 4.17: Sketches of the first prototype concept.

***Concept 2: Integrated reflective ramp***

The second concept was generated using the solutions underlined with green in Table 4.2. This concept makes use of the shape of the body to create a strain relief effect. The holes through which the fibre tubes run are made slightly smaller than the size required to fit the four fibre tubes through the hole smoothly. This is done by creating a flattening inside of the semi-circles that together form the hole for the fibre tubes. This is illustrated in Figure 4.18. By making the hole slightly smaller, the fibre tubes will be slightly compressed when they are run through the body. Therefore, the fibre tubing acts as a spring and a higher normal force will exist thus creating higher friction. As opposed to Concept 1, the fibres run internally through the tip to their respective positions. For sensing sideways, a similar method is used as was described in Concept 1. A reflective surface is created on top of a 45° ramp to reflect the light perpendicular to the surface of the device tip. A wall is placed in the middle of the ramp to prevent the light from directly entering the collecting fibre.

In the tip, two holes are drilled so the forward-facing fibres can be inserted at the required core-to-core distance. This is done while keeping the wall thickness between the fibre and the outside of the tip to a minimum.

To protect the fibres from wear, a clear adhesive is used. The notch through which the light will be emitted on the side is filled using this adhesive to cover both the reflective surface and the actual fibre tips. This way the fibres are constrained and cannot be moved out of their place. At the front of the tip, the two fibres are placed such that their ends do not reach the end of the tunnel by a tiny margin. By applying the adhesive into the holes a clear plug is created without having adhesive sticking out of the hole which could diverge light in an unwanted way.

By integrating both the strain relief function and the body design into one element, the number of separate elements in the design can be kept to a minimum which is advantageous during prototyping. Moreover, the strain relief can be easily adjusted by increasing or decreasing the length of the body, without the need for other adjustments elsewhere.

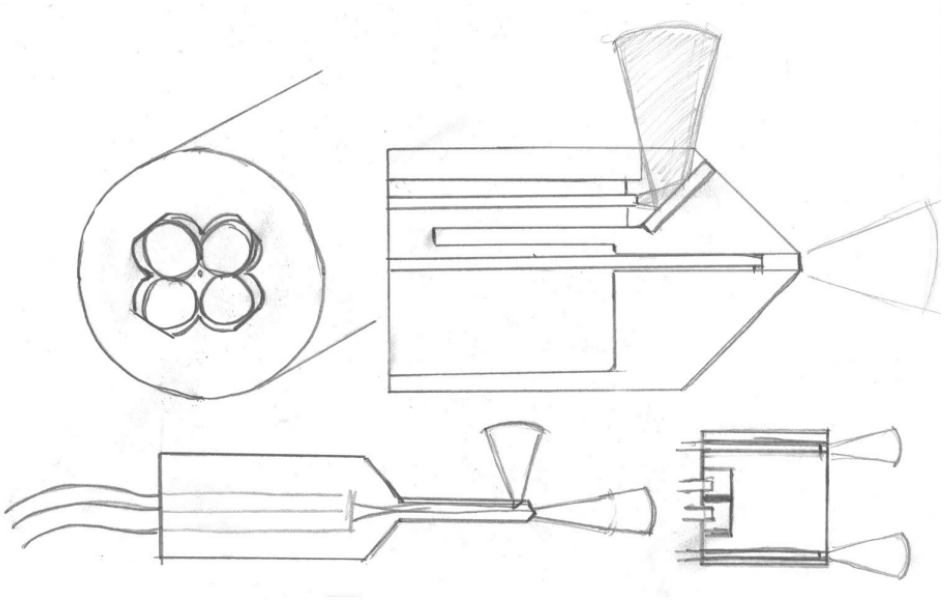

Figure 4.18: Sketches of the second prototype concept.

***Concept 3: Slanted fibre tip***

For the third concept, the solutions underlined with blue in Table 4.2 were used. Sketches were made for the concept and are shown in Figure 4.19. In this concept, a wedge is used to act as strain relief. The fibre tubes are laid in a single hole that runs along the length of the body. At the entrance of the body, the diameter of the hole gradually increases. This is done to create more space to incorporate the wedge inside the body. The wedge has a cone shape and is inserted in the middle of the four fibre tubes. This way the wedge pushes the tubes into the surrounding walls and secures itself. The wedge needs to be self-locking in order to stay in place. Nevertheless, to ensure that the wedge stays in place when an external force is applied to the fibres, a threaded cap is placed at the entrance of the tube to constrain any type of motion from the wedge. In case of the wedge creates insufficient friction when manually applied, the threaded cap can be used to apply force on the wedge, which creates a higher normal force between wedge and tubes, and thus more friction.

For the tip of this design, a similar structure to the one described in Concept 2 was used. Both the frontal and sideways sensing fibres are placed in a similar fashion. However, the light is reflected off the slanted tip of the fibre. As light travels through the fibre and arrives at the slanted interface, depending on the angle of the incident light and material properties of the interface, two things can happen. One part of the light is reflected upwards and refracts at the surface of the tip's core. This means the light exits the fibre at an angle. The other part of the light directly refracts on the slanted interface and continues into the instrument. Part of this 'lost' light could be recovered by using a reflective coating to reflect the light outwards. This is illustrated in Figure 4.14b, where the yellow line represents the internally reflected light and orange the light refracted at the internal interface.

The slanted fibre will only need to be orientated correctly with the slanted surface facing towards the centre of the instrument's tip. This means that no additional reflective structure needs to be incorporated into the tip compared to solution C2-2. However, the orientation of the fibre's tip is critical for the correct emission of light.

The use of glue helps to properly secure and protect the fibre tips. Although a silica cover would have been a suitable alternative, the slanted fibre tips can be placed at a relative low depth to the surface of the tip. Therefore, little room is left to incorporate a piece of silica while a drop of glue can be easily applied.

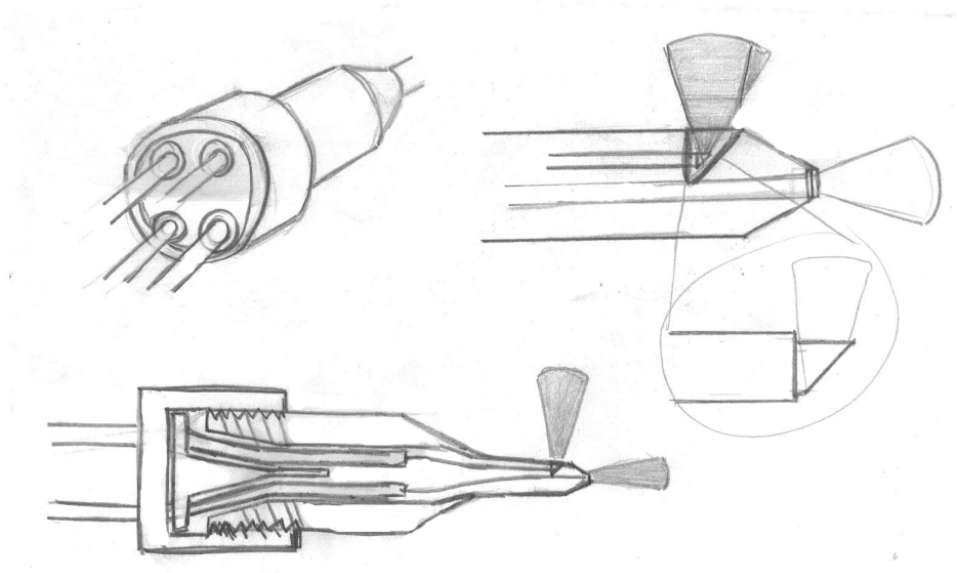

Figure 4.19: Sketches of the third prototype concept.

## 4.4. Concept scoring

To determine which concept is the most suitable, a Harris profile was made. A Harris profile was chosen as it shows the strengths and weaknesses of a design concept with respect to a set of criteria [44]. However, it does not rely on a set of data to be used. This profile gives a general overview of the concept to the designer and does not provide any quantitative information. The criteria used in the Harris profile together with their respective grading method are listed below. The criteria are listed from most to least important.

1. *Drill ability* - The amount of force needed to use the tip as a drill. Less force is better.
2. *Device diameter* - The size of the device's tip is crucial in order for it to fit in the pedicle. The smaller the diameter of the tip, the better.
3. *Assembly* - The ease by which the prototype can be assembled. Easier is better.
4. *Fibre protection* - The amount of risk the fibres have being damaged during the use or assembly of the device. Less risk is better.
5. *Fibre security* - How secure are the fibres mounted on to the device. The more secure the fibres are, the better.
6. *Bending stiffness* - The ability of the tip to resist bending when a load is applied on the tip during drilling. Higher bending strength is better to prevent bending.

Looking at the Harris profile in Figure 4.20, it can be seen that Concept 1 scored better on the first two criteria which are also the most important criteria. However, the drill ability is mainly influenced by the device diameter. Furthermore, Concept 1 does not do well on assembly and fibre protection. The actual difference in diameter between Concepts 1, 2 and 3 is small. Moreover, Concept 2 scored overall better in the middle part of the table while the three concepts score similarly in the lower half of the table. In addition, Concept 2 is the only concept that scored positive on all criteria. Therefore, the decision was made to choose Concept 2 and continue to develop this concept further into a prototype.

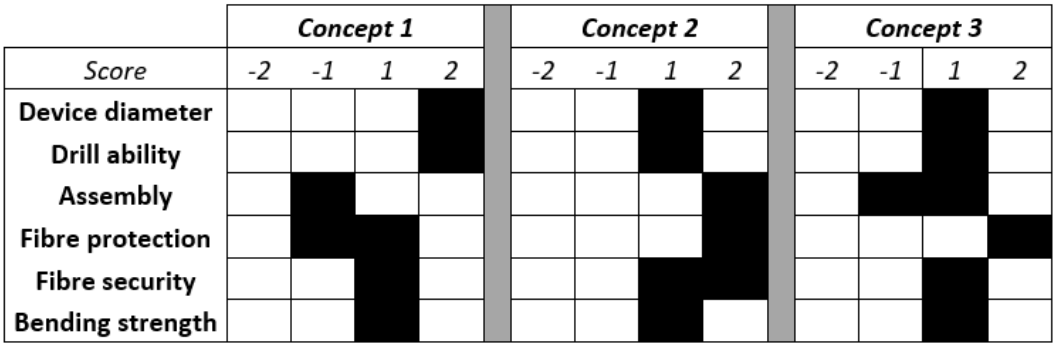


Figure 4.20: In the Harris table, the scoring of the concepts is shown with regard to the set of requirements listed on the left.

## 4.5. Final design

### The components

Based on the solutions used in second concept, rapid prototyping was used to design, review and refine a design for a prototype. By making use of fused deposition modelling (FDM), a type of 3D printing, multiple iterative cycles were done to obtain a working prototype that could be easily assembled. The prototype is made out of four separate components, consisting of a body, a connector and two halves of the tip. This build-up was used for two reasons. First of all, by making the prototype of separate parts, the individual parts can be refined individually without the need for reprinting the whole prototype. It helped in keeping the iterative process efficient. Secondly, by making the design modular the assembly of the prototype was made easier without a large risk of damaging the wires. If the prototype would have been one component, mounting the fibres in their respective places would have been more difficult due to hole sizes.

### Body

In Figure 4.21a, a top view of the final design of the body is shown. At the front of the body, a decrease in diameter can be seen. This reduction was incorporated into the design to mount the connector that is used to keep the tip and body together. The hole that can be seen in the front section of the body is used to secure the connection component to the body. This is done by inserting an M2 screw through the connector into the body.

As mentioned before, the body has two functions. It will be responsible for both strain relief and guiding the fibre tubes to the tip. In Figure 4.21b, an axial cross-section from the body can be seen. The four fibre tubes are inserted through the middle where each fibre tube has its own groove. The grooves along which the fibre tubings lay are made slightly smaller than the diameter of the tubing, by around 0.1 mm. This can be seen in Figure 4.21b, by the flat areas in the semi-circular grooves. This reduction in diameter helps press fibre tubes together and lock them in place against the surrounding walls of the device, effectively wedging themselves. Therefore, an external force applied to the wires can be absorbed by the friction produced between the tubing and the surrounding walls. By integrating Parts A and B from Figure 4.1 into a single part while maintaining the functionality of both parts, it has the advantage of facilitating the assembly.

(a) (b)

Figure 4.21: In (a), a top view of the prototypes body. In (b), the cross-section of the body. The clover-like shape will contain the fibre tubing.

Figure 4.22: On the left, a top view of the connector. On the right, the cross-section of the connector. For the cross-sectional view, the connector was turned 90° to show the holes used for securing the connector to the body.

## Connection

Because of the modular design of the prototype, the tip and the body are separate parts. A connector was designed to ensure a proper connection between the tip and body. This connector can be seen in Figure 4.22. The connector is a hollow cap which will encapsulate the ends of tip parts. After both tip parts are inserted through the connector, the connector can be slid over the section of the body with a reduced diameter. If the connector is fully mounted, the body is in contact with the end of the tip. Therefore, the connector pushes the tip into its correct position and locks any movement from either half of the tip.

The screw holes in the connector line up with these present in the body. Inserting M2 screws ensures that the connector cannot move anymore. To regain access to the fibres inside the prototype, the screws are removed and the connector can be pulled loose.

## Tip

The tip is split into two separate parts as manual insertion of the optic fibres is a difficult task due to the small dimensions. The parts can be seen in Figure 4.23, consisting of the blue, orange and green parts. The blue part contains the reflective material (green) that is needed for sideways sensing. As shown in Figure 4.23b, two parallel grooves (yellow-solid) run along the right of the blue part. The optic fibres used for sideways sensing enter the tip at the right and run along the inner wall, through these grooves. The fibres are inserted into the holes at the end of the grooves which will place the fibres in front of the reflective surface (yellow-dotted). The reflective surface was made using a piece of metal flexure that was manually cut to the right size. The surface of the metal was left untreated to not influence the scattering property.

The other two fibres run to the front of the tip where they are laid inside the grooves that run from the front of the tip. These grooves guide the fibres to their correct place and are indicated with the black lines. During the testing and assembly of the device, it was noticed that the optic fibres were difficult to handle due to their lightweight and fragile nature. Small movements made during the process resulted in the fibres moving before the prototype could be fully assembled.

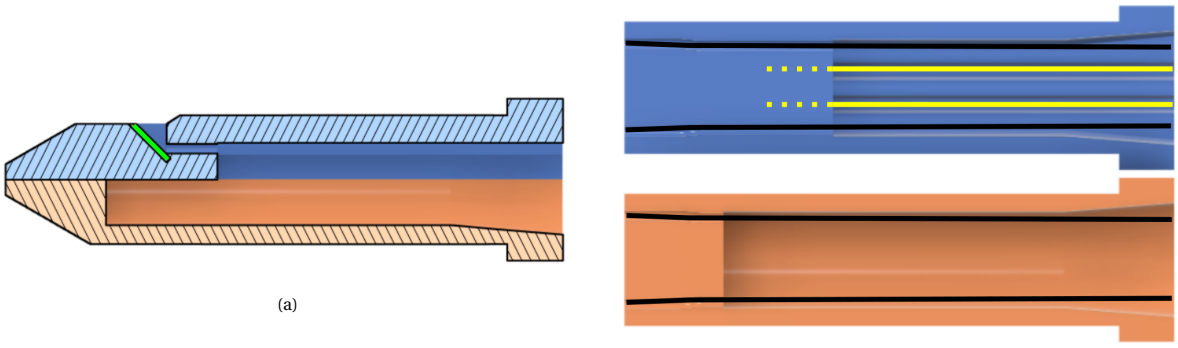

(a) (b)

Figure 4.23: On the left, a cross-sectional view of the tip. The blue and orange halves are separate parts. On the right, the inside structure of both halves of the tip is shown. The yellow and black lines indicate the position of the optical fibres.

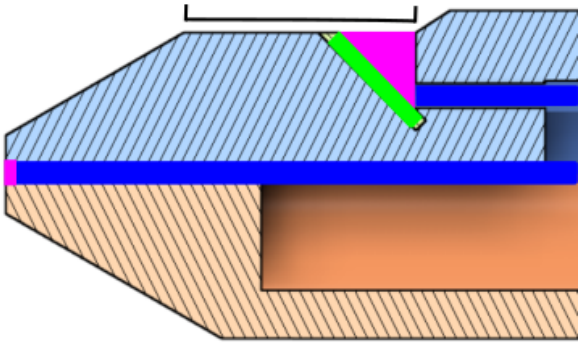

Figure 4.24: A close up of the tip of the prototype. The dark blue lines correspond to the optic fibres, the green line represents the reflective surface and purple indicates where the adhesive is applied.

To solve this problem, malleable rubber was used as a temporary adhesive. Other types of solutions for securing the fibres were considered such as clamping or glueing, however, these did not have the same flexibility as the malleable rubber. The malleable rubber could be shaped according to the inside of the tip and was used to secure the fibres. The advantage of using this type of adhesive over other types is that the rubber-like material does not cure and the amount of material that is used can be quickly adjusted. This means that changes can be easily done during assembly and the fibres are not stuck in place. In Figure 4.24, a cross-section of the front of the tip is shown. The pink areas show where the adhesive is used to close the holes through which light is emitted and collected.

To seal the holes and protect the fibre tips, an adhesive is used that is near-transparent in the near-infrared range. The adhesive, called NOA81 by Norland Products(USA), cures when exposed to UV light and it will form a hard and clear polymer. Figure 4.25 shows the spectral transmission of the cured glue. The adhesive is near-transparent in NIR, between 1000 and 1800 nm.

The curing process was done after the prototype was assembled. The prototype was placed in a UV curing device from Formlabs (USA). As the UV wavelength of the UV curing device was slightly off the recommended wavelength for curing, the curing time inside the machine was increased to compensate.

In Figure 4.24, a flat surface on top of the blue area is indicated using a black line. This flat area was made on the side of the cylindrical tip to help the adhesive form a flat surface. In a previous iteration, the reflective surface was partly incorporated in the tapered surface of the tip. This caused the adhesive to form a curved surface, thereby reflecting light at a wrong angle. During the testing, the sideways light was not emitted at a 90° angle but more backwards. The flat area at the tip helps to keep the adhesive level during curing and forms a flat surface during the curing process.

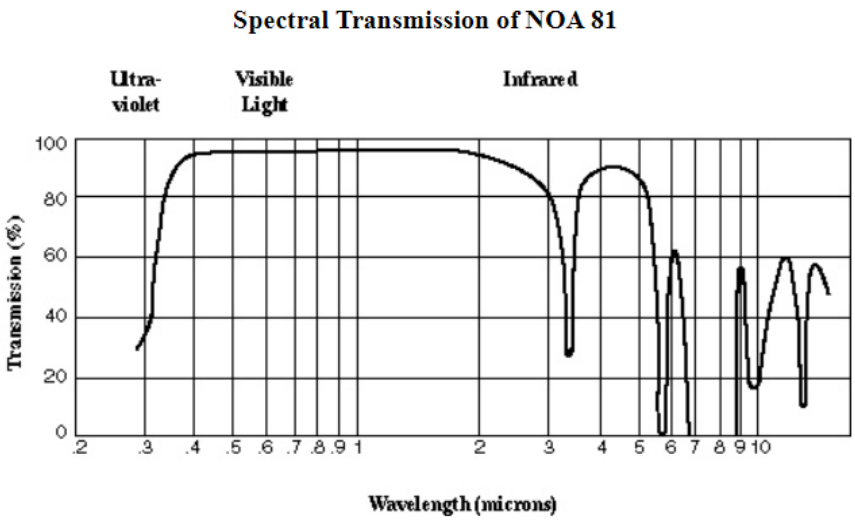


Figure 4.25: In the figure, the spectral transmission of NOA81 after curing is shown.

## 4.6. The prototype

### Assembly

The actual prototype was 3D printed using fused deposition modelling on an Ultimaker 3. The material that was used is polylactic acid (PLA). This material was chosen as it is easy to print and strong enough to be used for drilling into an optical bone phantom.

In Figure 4.27, all the different components can be seen. The assembly was done in multiple steps. First, all the fibres were inserted into the body (purple) till the fibre tubing reached the end of the body. Next, the optical fibres for sideways sensing were inserted into the tip half that contains the reflective ramp (blue). The two fibres were laid along their respective grooves till the tips were inserted till the ramp. The two fibres were then secured using the reusable adhesive.

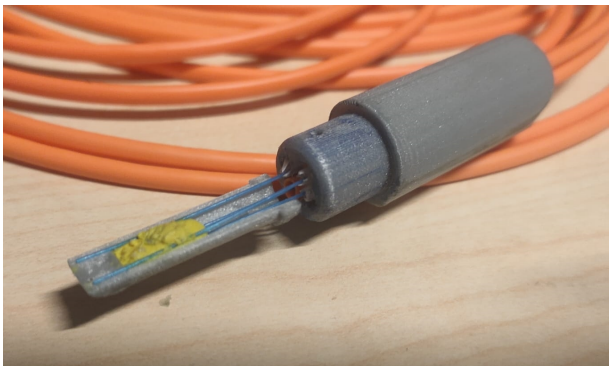

Figure 4.26: The prototype in a half assembled state. The blue lines are the optical fibres. The yellow material is malleable rubber used as adhesive for the optical fibres.

The forwards sensing fibres were then laid in their respective grooves and secured as well. This can be seen in Figure 4.26. After all the fibres were in place the other half of the tip (orange) was put in its corresponding spot, thereby closing the tip of the instrument. To secure the tip in place, the connector (red) was inserted over the tip. The last component that was inserted was the piece of metal that acts as a reflector for the light. After it was placed, the clear adhesive was applied over the ramp and on both the forward and sideways fibre tips. The adhesive was cured using a UV curing chamber for twenty minutes.

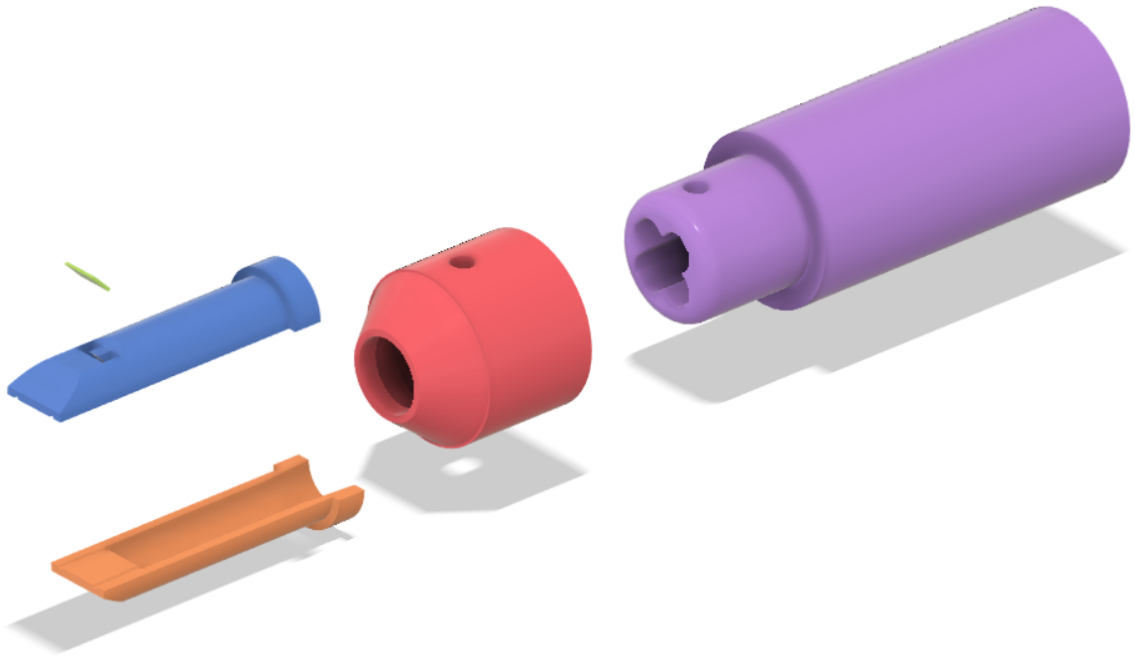

Figure 4.27: An exploded view of the prototype.

## Finished prototype

The actual prototype can be seen in Figure 4.28a. It can be seen that the dimensional requirements are met. The outside diameter of the device is 6 mm which means it is within the required range of 6 mm and smaller. If the LAD exceeded the expected value, it means that the diameter of the tip can be further reduced making it possible for use in smaller vertebrae.

Furthermore, the bending radius of the optic fibres does not exceed the minimum stated value as no bending was used to emit and collect the light sideways. In addition, the length of the drill is 2.1 cm and thus exceeds the minimum of 1.5 cm length of the requirements. The other dimensions can be found in Figure 4.28b.

Preliminary testing indicates that the prototype is able to drill through the optical bone phantom easily. However, no tests were done on a bone phantom that replicated the mechanical properties of cancellous and cortical bone. The material requirement is not met as the design is made of PLA. However, this should not limit the prototype during testing.

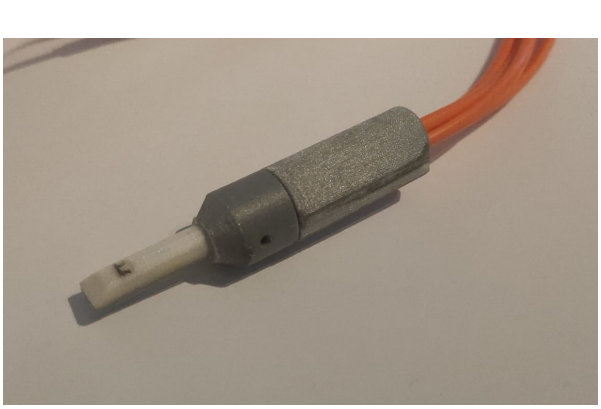

(a)

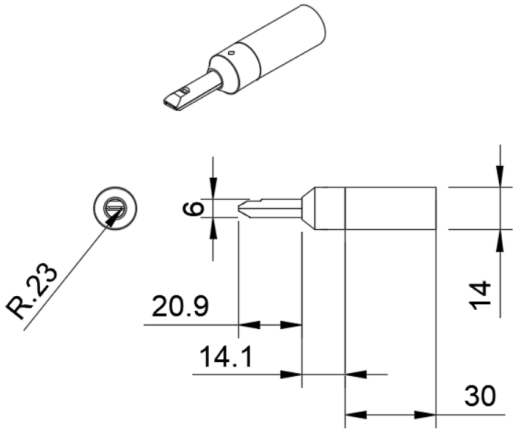


(b)

Figure 4.28: In (a), the assembled prototype is shown. The orange cables are the optical fibre tubing going into the prototype. In (b), the dimensions of the prototype are given (in mm).

# 5

# Testing of prototype

## 5.1. Goal

The performance of the prototype needs to be tested to find the look-ahead distance (LAD) of both the forwards and sideways sensing fibres. The LAD determines if the prototype can provide directional feedback and thus guidance. This is done to ensure the prototype's LAD is in line with the predicted LAD and see if the guidance requirements are met. Based on the results a statement can be made on the prototype's ability to provide directional feedback for a user.

Two independent experiments were done to validate the design. The first experiment was done to check if the frontal sensing capability of the prototype has the expected LAD. The second experiment was done to test if the sideways sensing mechanism worked as expected and the expected look-ahead distance was obtained. Furthermore, the prototype is also checked on the other requirements listed in Section 2. These requirements consider the other properties that are important to the functionality of the prototype.

## 5.2. Method

### 5.2.1. Experiment 1: Forward look-ahead distance

For Experiment 1, a two-layered optical bone phantom was made. The top layer replicated cancellous bone and the bottom layer resembled the optical properties of cortical bone. The cancellous bone was used as top layer as this is the bone type in which is drilled during a procedure and because the cortical layer needs to be detected through the cancellous bone. To produce the optical bone phantom, first the cortical layer was made. The fat content of cancellous bone (34%) was replicated using porcine fat which was added during the fabrication of the cortical layer. Porcine fat is used as this type of fat is similar in structure to human fat [45]. The other materials and their quantities which were used for the production of both layers can be found in Table 5.1. Distilled water was added to replicate the water content in bone. Sodium chloride was added to provide some electrolytes. Sodium benzoate was added as preservative agent and barium sulfate acts as a scattering agent. Gelatin was added as emulsifier and also acts as gelling agent.

The cortical layer that was made is the same as used in the validation of the simulations. The cancellous layer was made by heating the water on a hot plate stirrer to 50 °C. The NaCl, sodium benzoate and barium sulfate were dissolved. Gelatin was added and the mixture was heated to 70 °C. The fat was separately heated till it turned liquid and added to the mixture while stirring at 550 rpm. The heat was turned off while the mixture was stirred. When it reached between 40 °C and 50 °C, the fluid was put into a mixer to be shortly mixed. This was done to properly mix the gelatin and fat to obtain a homogeneous mixture. The phantom was then poured on top of the cortical layer and cooled in the freezer till solid after which it was placed in a refrigerator.

Table 5.1: Materials used in the cancellous layer of the bone phantom.

| *Layer* | Cancellous |
|---|---|
| *Fat (porcine)* | 34 ml |
| *Water* | 66 ml |
| *NaCl* | 0.66 g |
| *Sodium Benzoate* | 0.066 g |
| *Barium Sulfate* | 0 g |
| *Gelatin* | 9.9 g |

Before the experiment, the bone phantom was taken out of the refrigerator. This was done to let the phantom warm up to room temperature, so it better resembles the temperature of the vertebrae inside the body.

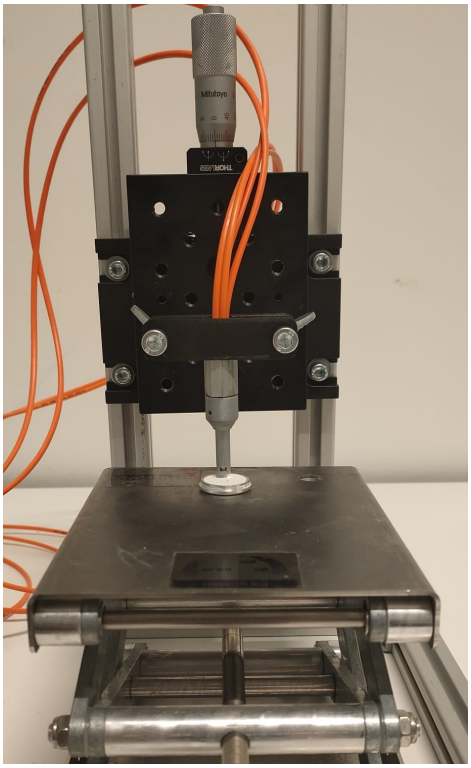

Figure 5.1: The setup used during experiment 1 is shown.

Next, the DRS console was calibrated according to the way described in the standard manual. The first two calibration steps are done internally by the DRS console. For the final calibration, the console was calibrated to the prototype. The fibres corresponding to the frontal sensing part of the prototype were connected to the DRS console. The calibration was done according to the same calibration steps as described in Section 3.5. The testing room was darkened to avoid external light from influencing the reflectance data.

The two-layered bone phantom was placed beneath the prototype on an adjustable platform with the cancellous layer on top. The prototype was positioned at a 90° angle, with the device's tip pointing downwards. The prototype is mounted onto a moving stage. The stage has a step accuracy of 0.01 mm (Thorlabs Inc. USA). The setup used during Experiment 1 can be seen in Figure 5.1 The platform's height was increased till the surface of the phantom was in contact with the front of the prototype's tip. After the contact was made, only the stage was moved.

After a measurement was done, the prototype was lowered into the bone phantom. The prototype was lowered into the phantom based on the distance between the prototype and the cortical layer. As the distance decreased, the step size was decreased to obtain a better resolution of the LAD near the cortical layer. The step sizes that were used are shown in Table 5.2.

Table 5.2: This table contains the step sizes used for moving the prototype into the bone phantom during the experiment.

| **Distance to cortical layer** | **step size of stage** |
|---|---|
| *11 mm to 5 mm* | 1 mm |
| *5 mm to 1 mm* | 0.2 mm |
| *1 mm to -1 mm* | 0.1 mm |

### 5.2.2. Experiment 2: Sideways look-ahead distance

The goal for Experiment 2 was to test the sideways sensing fibres and measure its look-ahead distance. Therefore, a different setup was used as the prototype could not be lowered through the bone phantom sideways. This was not an option as the bone phantom does not respond well to the application of force over a bigger area, as was found during the validation experiment. A custom mould was printed in which the two-layered bone phantom was cast. This mould can be seen in Figure 5.2. The mould has holes in its sides through which the prototype can be inserted horizontally. This allowed the measurements to be taken at specific heights above the cortical layer. The height difference between each of the holes was 0.25 mm. The mould had a circular shape to lower the amount of material needed for the bone phantom. The mould's diameter was chosen so that the prototype would not have to be inserted inside an area of the bone phantom that had been measured before. This prevented the bone phantom from tearing. The prototype was horizontally mounted in a clamp. Its height was not adjustable. Therefore, an adjustable platform was used to move the mould vertically.

Before the experiment, the bone phantom was taken out of the refrigerator, and the sideways sensing fibres were connected to the DRS console. The same calibration process as described in section 3.5. However, the prototype was placed horizontally above the spectralon during the third calibration. This was done as the sideways sensing fibres needed to have a direct line of sight of the spectralon for the calibration.

After the calibration, the entire length of the prototype's tip is horizontally inserted into the mould containing the bone phantom. This is done to ensure the inner walls of the mould are as far away as possible from the sensing area of the sideways fibres. If the walls are detected, the collected data will be influenced, which is not desired. After each measurement, the platform is lowered, and the insertion is done again. In addition, by inserting the prototype into the mould till the outer walls of the mould touch the connector, the contact ensures that the mould is horizontal.

The measurements were done starting with the top hole and descending after that. The bone phantom can easily tear when the prototype is inserted as the holes are relatively close. The bone phantom that has torn can move when inserting the prototype. Commencing the experiment from top to bottom ensures that the measurement is done in a solid part of the bone phantom. During each insertion of the prototype, ten measurements were done.

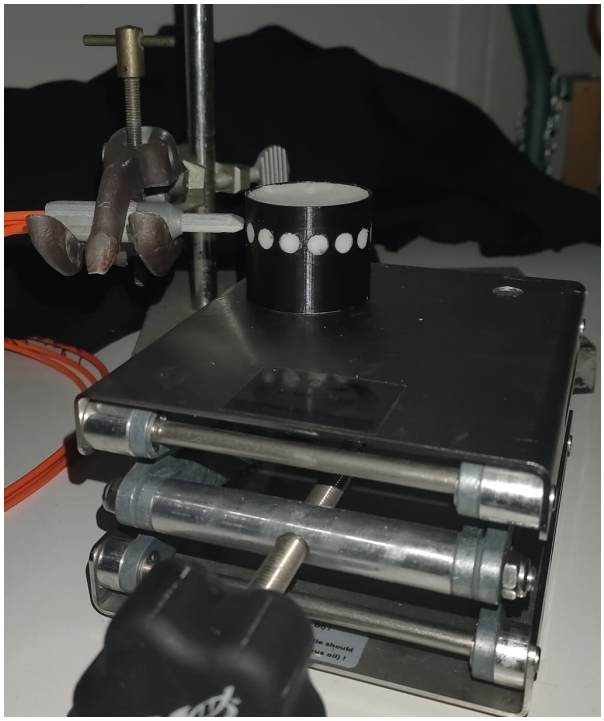

Figure 5.2: The setup used during experiment 2 is shown.

### 5.2.3. Data processing

For both experiments, the collected data was processed using Matlab. The ten spectra that were collected at each measurement point were averaged to obtain an average reflectance spectrum. The averaged reflectance spectrum was then filtered using a moving average filter with a window of five to make the data better readable. These filtered data were scaled to the measured intensity at a wavelength of 1200 nm, the wavelength at which light is absorbed by fat. The data was plotted against the range of wavelengths emitted by the DRS console.

## 5.3. Results

### 5.3.1. Experiment 1: Forward look-ahead distance

The reflectance spectra of Experiment 1 can be seen in Figure 5.3. Every reflectance spectrum at an increment of 1 mm above the cortical layer is shown to make the curves distinguishable. The measured intensity decreases as the probe approaches the cortical layer. By looking at Figure 5.3, the look-ahead distance is difficult to extract from the curves. To facilitate the LAD extraction, the intensity at the wavelength of 1200 nm was taken from each reflectance spectrum and plotted against the distance of the prototype to the cortical layer of the bone phantom. The wavelength of 1200 nm was chosen as the fat inside the phantom absorbs light of this wavelength.

In Figure 5.4, the results of both measurements of Experiment 1 are shown. The data of both measurements behave similarly, as the intensity during both measurements decreases as the prototype moves closer to the cortical layer, which is located at 0 mm. Eventually, the intensity for both curves becomes constant, which means the prototype has entered the cortical layer.

The decrease in intensity starts at 3.2 mm for Measurement 1 and 3.2 mm for Measurement 2. Thus, the LAD for the forwards sensing fibres amounts to a minimum distance of 3.2 mm for a core-to-core distance of 4 mm.

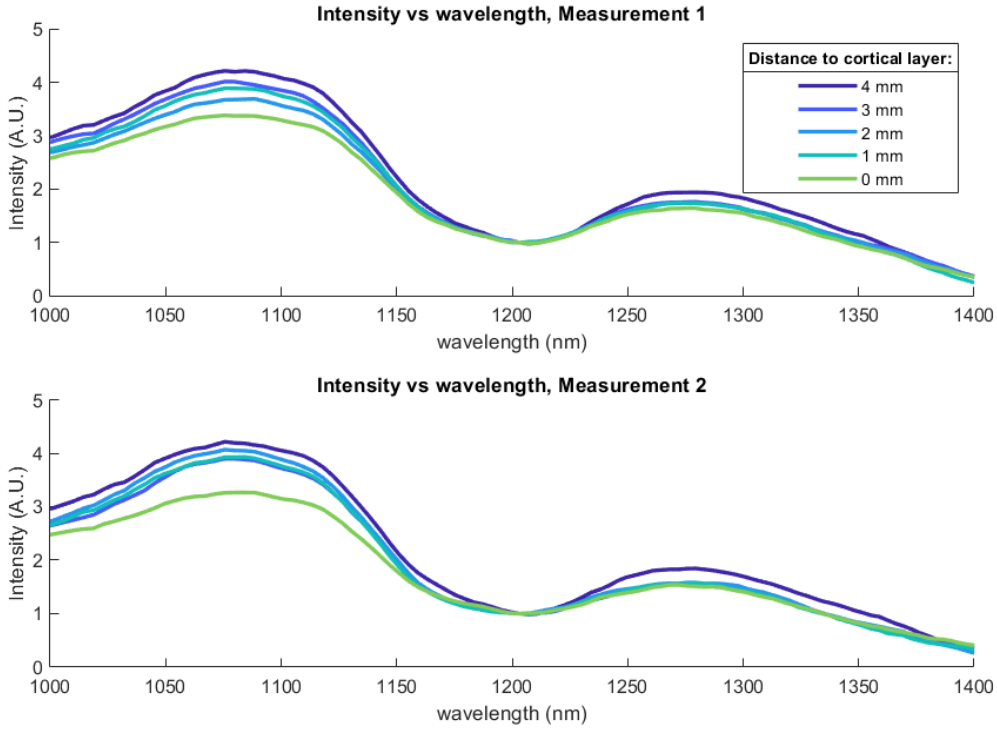


Figure 5.3: The reflectance spectra for both Measurement 1 and Measurement 2 were collected at different distances from the cortical layer inside the bone phantom. The forward sensing fibres were used to collect the spectra.

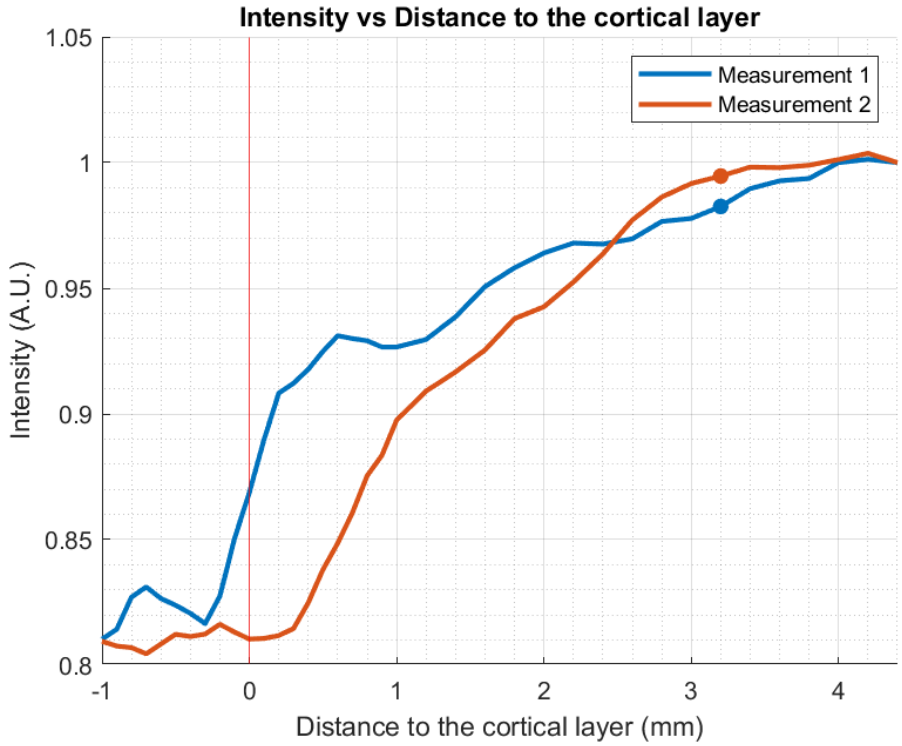


Figure 5.4: The intensities measured during both measurements were plotted for different distances from the cortical surface for the frontal sensing fibres. The intensities were collected for light with a wavelength of 1200 nm.

### 5.3.2. Experiment 2: Sideways look-ahead distance

In Figure 5.5, the spectra from a single measurement are plotted. The other measurement did not produce any results that could be interpreted sensibly; therefore, it was omitted from the results. The intensity data was scaled to the wavelength of 1200 nm, the wavelength at which fat absorbs light.

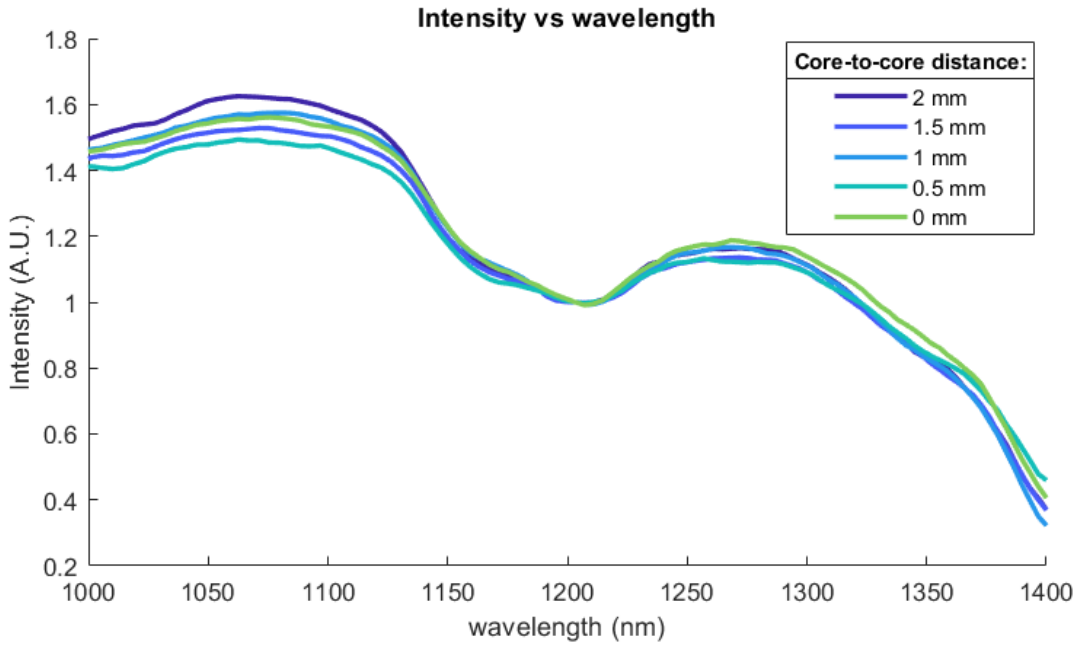


Figure 5.5: The reflectance spectra that were collected at different distances from the cortical surface. The sideways sensing fibres were used to collect the spectra.

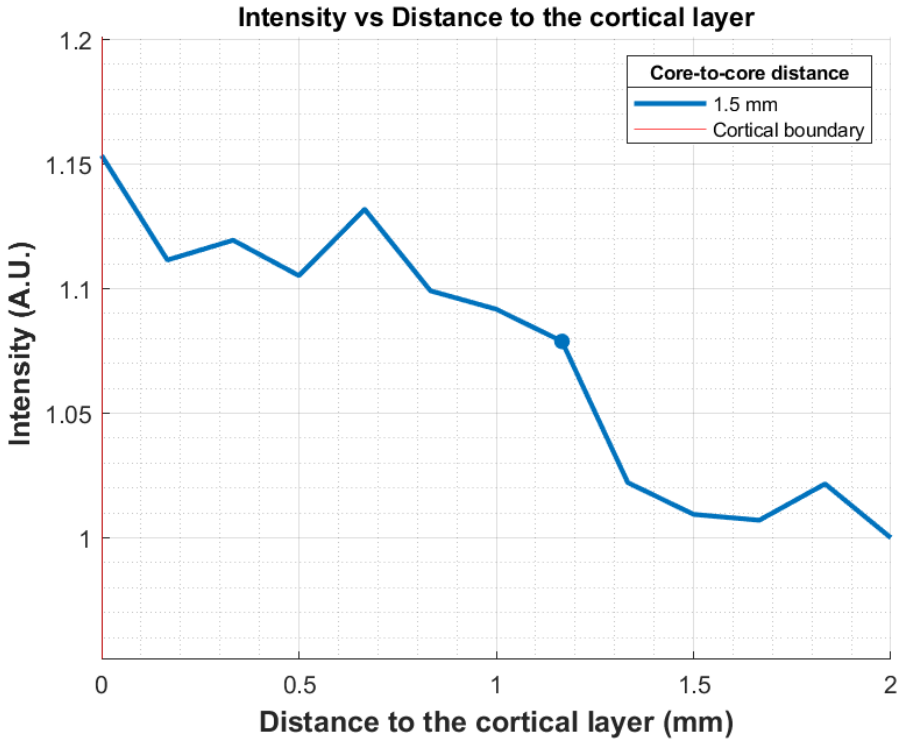


Figure 5.6: The figure contains the measured intensity for a wavelength of 1200 nm versus the distance from the cortical layer.

In Figure 5.6, the intensities for the wavelength of 1200 nm are plotted against the distance to the cortical layer. The intensity increases as the distance to the cortical layer decreases. This behaviour is in line with the simulated and experimentally obtained LADs. A LAD of around 1.2 mm can be extracted from the curve.

## 5.4. Discussion

Multiple observations can be made from the measured intensities in Figure 5.6 for Experiment 1. Firstly, the LAD of the forward sensing fibres of 3.2 mm is more than the expected LAD of 2.8 mm. This is an increase of 23% The LAD is still within the expected range as a core-to-core distance of 4 mm was chosen to fulfil the requirement of a minimum LAD of 2 mm. As the measured LAD is larger than expected, one can assume that the core-to-core distance can be reduced while maintaining a sufficiently large LAD that meets the requirements. Nevertheless, the deviation is significant. Comparing the setup of Experiment 1 and the setup used to validate the simulations, a difference is the material used for the cancellous bone and the probe. The simulation validation experiment used coconut milk instead of the optical cancellous bone. Therefore, the consistency of the phantom and the fat content may have influenced the LAD, although the liquid mixture was mixed to create a homogeneous mixture. Another explanation could be that the optical fibres in the multi-fibre probe have other properties.

Based on the decreasing intensity when the probe approaches the cortical layer a more likely possibility is an error in the initial height above the spectralon during calibration. This could have resulted in the decrease in intensity when approaching the cortical layer as opposed to an expected increase. Despite these possible explanations, Figure 5.4 shows a clearly defined decrease in intensity at a certain distance from the cortical layer which stops when the cortical layer is reached.

The measured reflectance by the sideways sensing fibres is as expected as it increases as the probe approaches the cortical layer. The core-to-core distance of 1.2 mm is in the region between 1 and 2 mm where the detected intensity transitions from decreasing into increasing. This is similar to the intensity measured in the experiment that validated the simulation results.

Lastly, the difference between the LAD measured in Experiments 1 and 2 is 0.6 mm, which is significant considering that the bone phantom was not changed. This difference could be explained by the fact that the surface of the bone phantom and the boundary between the two layers of the bone phantom are not flat. As the measurements were done on different locations in the phantom, the surface's minor deviations could

account for the difference in LAD. However, this does not explain the difference in slope during the decrease in reflectance between 2 and 4 mm that can also be observed in Figure 5.4. The slope in Measurement 1 is less than the slope in Measurement 2. An explanation could be that the local fat content at the location of both measurement was not equal.

# 6

# Discussion

## 6.1. Main findings

### Introduction

This thesis presents the design for a guidance instrument that users can manually use for drilling inside the pedicle. The device uses diffuse reflectance spectroscopy (DRS) as a sensing mechanism. The device emits light and collects the reflectance spectra inside the bone, thereby sensing the distance between the device and the cortical wall in axial and transverse direction. The drilling direction of the instrument can be adapted based on this directional feedback.

The results obtained by testing the actual prototype indicate that the forwards and sideways sensing fibres work as intended.The forwards LAD was measured at 3.2 mm while the sideways LAD was 1.2 mm. The required LADs are both reached; thus, the device can detect a sufficiently large volume. This means that the distance to the cortical wall can be provided by the instrument, which is the directional feedback that can provide guidance.

### Simulations

The use of simulation software showed to be a valuable addition. It provided a fast method of testing out multiple core-to-core distances to obtain a first impression of the LAD inside the cancellous bone for larger core-to-core distances than were reported in the relevant literature. The simulation of larger core-to-core distances was relevant as originally, DRS is not used to detect a certain distance inside tissue but for spectral analysis of a sample. The first simulation results indicated that it was possible to meet the required LAD of 2 mm for forwards sensing. Based on the simulations and validations experiment, core-to-core distances of 4 mm and 1.5 mm were chosen for frontal and sideways sensing, respectively. These distances were chosen as their corresponding LADs are larger than the required LAD, while meeting all requirements regarding the diameter of the device.

It should be noted here that although this core-to-core distance results in a diameter slightly larger than 4 mm, the diameter is still within the limit set for the diameter. Still, a smaller diameter would be advantageous to facilitate drilling by hand or provide access to smaller pedicles in other parts of the spine.

### Forwards look-ahead distance

Based on the validation experiment and the simulations, a frontal core-to-core distance of 4 mm was chosen to meet the minimal required LAD of 2 mm. A core-to-core distance of 3 mm is also sufficient according to the validation experiment. However, the sample size of the measurements done was too small to accurately ensure this core-to-core distance. Furthermore, the axial direction is more at risk for perforation as this is the drilling direction. The users drill by hand, and thus they are more likely to overshoot in the axial direction. A smaller LAD is applicable for the sideways sensing capability as the instrument's body is not expected to move in transverse direction. In addition, a LAD that reaches beyond the pedicle wall is not necessary.

The LAD found experimentally for forwards sensing of the prototype was 3.2 mm. This is an increase in the forward LAD of 14% compared to the LADs obtained from the simulations and the preliminary validation experiments. In itself, the increase in LAD is positive as it means that a larger LAD is obtained without an

increase in the diameter of the device and thus effectively increasing the instrument's functionality. However, the inability to predict this increase based on the simulations and validation is unexpected. The larger number of photons during the measurement could be responsible for the larger than expected increase of the LAD. A difference in the properties of the optical fibres that were used such as a different numerical aperture or core diameter of the fibre could also have resulted in the difference in LAD.

### Sideways look-ahead distance

The sideways LAD of the prototype shows a decrease in LAD compared to the validation experiment, with the LAD being smaller than the measured LAD for a 1 mm core-to-core distance. Two possible reasons were identified. Firstly, the decrease in intensity measured for the core-to-core distance of 1 mm and the subsequent increase of intensity for the 2 mm core-to-core distance means that core-to-core distances between 1 and 2 mm could experience unwanted fluctuations in the intensity. This does not seem to be the case for the sideways looking fibres as increase in intensity is measured. However, a minor increase in intensity could have been the result of this transition zone between the core-to-core distances of 1 and 2 mm, thus resulting in the smaller LAD than expected.

Secondly, the predicted and validation LAD were based on a perpendicular fibre to the measured medium and did not consider a reflective surface. In addition, the fibre tips were near the phantom in the case of the validation experiment. However, for the prototype, the light must first be reflected from the metal surface and make its way to the surrounding tissue and vice versa for collection. This could decrease the amount of collected light compared to the frontal sensing fibres and thus result in a lower LAD than the predicted LAD. However, this does not seem likely as this should be included in the calibration.

Another reason for the decrease in LAD could be the ramp that reflects the light sideways. Essentially, it is harder for the light to reach the collecting fibre as it needs to traverse a longer path due to the 270° turn it needs to make compared to the light emitted from the forwards sensing fibres. This latter reason seems most likely as the switching increase and decrease of intensity between 1 and 2 mm should only increase the difficulty of a detectable point and not decrease the LAD.

### Prototype versus PediGuard

The prototype can be compared to other similar instruments such as the PediGuard. The PediGuard is a medical instrument that can be used for drilling into the pedicle by hand. It provides feedback based on tissue conductivity which is measured at the tip of the device. The prototype made for this thesis has some clear advantages compared to the PediGuard: during the use of the PediGuard, constant pressure needs to be applied to the device. This prevents blood from flowing into the hole, so the PediGuard does not give a false breach signal [46]. For the prototype, intruding blood is not a problem as the blood does not impede the sensing ability. The influence of blood on the reflectance spectra can be calibrated for or filtered out, thus having no influence on the feedback that is given.

Furthermore, the prototype is made to prevent cortical breaches before they can happen. It does this by providing the distance to the cortical layer to its user. This allows the user to actively steer the prototype. The PediGuard can detect the transition of cancellous bone to cortical bone based on the change in the sound feedback. Williams et al.(2014) indicates that this change of sound lets individuals anticipate when to stop drilling to prevent a cortical breach [47]. Instead, the prototype should be able to give an accurate distance to the cortical layer without the need for anticipation. One should note that the PediGuard has proven its use during spinal surgery, where the prototype in question is still only a proof of concept. Nevertheless, the results of the prototype are promising for future application in the medical field.

## 6.2. Limitations

The research in this thesis has limitations in several aspects. The prototype provides directional feedback based on the light absorbed by fat inside the bone. However, the bone phantom is different from a natural bone in multiple ways. The bone phantom had a clear boundary between the first and second layers, where the fat concentration jumped from 17% to 0%. In natural bone, this 'hard' boundary does not exist between the cortical and cancellous bone as the fat content decreases gradually. This fat contrast in the phantom makes it easier to detect than a gradual fat transition. Research has shown that the decrease in fat content can be detected [3]; however, this prototype has a larger core-to-core distance with a LAD measured on a two-layered phantom. As it is not verified that this prototype has the same ability for transitional regions of fat, the LAD could be lower when used on human or porcine tissue. The performed experiments were stationary

and did not take any movement or turning into account. In addition, the prototype only senses sideways in 1 direction. Therefore, this prototype needs to be rotated around its central axis to sense the surrounding pedicle walls during drilling. In theory, this should not hinder data acquisition as the light source and the core-to-core distance are unchanged. If the effect is more significant than expected, it could disturb the prototype's guidance ability.

Rotating does introduce a problem regarding the optical fibres that are connected to the instrument and light source. Duperron et al.(2019) solved this by introducing a sapphire ball lens that allowed their drill bit to rotate independently from the optical fibres. Another potential solution would be to mount the light source on an axis that can rotate along with the optical fibres to prevent entanglement. This would keep the instrument less complicated and easier to assemble. Of course, a wireless solution such as the PediGuard would be preferable.

Multiple design decisions were made regarding the core-to-core distances of the prototype based on the simulation and validation experiment. After scoring the different concepts, one was chosen, constructed and tested. Although valid reasoning was used to select the current design, it does not mean that the other ideas and solutions are not viable. In addition, the prototype's performance can only be based on the requirements that were set up. As no other instruments exist that provide a similar directional feedback, bench marking the prototype is difficult.

Furthermore, the statement that directional feedback can be provided is based on the assumption that a suitable DRS console is used. The setup used in this thesis cannot give any actual real-time guidance. The information needs to be processed externally to obtain the distance to the boundary cortical.

In addition, the DRS console used during the experiments is not capable of using the front and side fibres simultaneously. Therefore, no tests were conducted using both fibre pairs simultaneously as the console can only emit and collect light using one pair of fibres.

Lastly, the data collected during the DRS measurement was not always consistent due to fluctuations in the measured intensity. Using the same probe, two similar measurements could provide two different measured intensities that had a significant difference and this could not be explained using either the used method or other observable events. The inconsistency was observed several times while using the prototype and during the validation experiment with a professional probe. To mitigate these outliers, the data was filtered using centered moving average filters. However, this does make the information less accurate in the way that the measured intensities will become higher or lower depending on the other measured intensities. Therefore, the extracted LAD could be lower or higher than the actual values would have predicted. Moreover, the method of LAD extraction gave varying results which does influence the decisions that were made based on these results. However, it was deemed better to keep the method of LAD extraction consistent for each set of data, than to make adjustments to individual results.

## 6.3. Recommendations

Some recommendations can be made based on the limitations mentioned earlier. Research can investigate the required look-ahead distance necessary for a user to react. This can help optimize the instrument further and reduce its size as the current prototype has still room for improvement in this aspect. The same data can be used to see the effect of the guidance of the prototype.

Furthermore, only a single concept was tested in this thesis. Although the current prototype works as intended, this does not mean the other proposed concepts would not have worked. Therefore, looking into alternative designs is beneficial as they have advantages as well. For example, for the sideways looking fibres, the slanted tip could potentially be used to reduce the sideways looking mechanism and simplify the design. In case the slanted tips do not produce the desired LAD, the design could still provide valuable information for further improvement of the current design. The slanted tips would help if multiple sideways facing fibres need to be integrated into the design. For the current design, modifications should be considered for sideways sensing. Changing the depth of the fibres to the surface of the probe could improve performance. Another research direction is to look into the requirements for a DRS setup that can integrate the information of multiple fibres and process the data in real-time. Eventually, this is necessary if the instrument is to provide directional feedback. Such a setup could also test the prototype and obtain the assumed directional feedback.

The detection depth of the instrument could also be utilized in other medical fields, especially for non-invasive methods. An interesting application would be to sample the blood inside the arteries and/or capillaries from outside the body by placing the instrument on the skin. For example, glucose could be measured

as it absorbs light in the NIR [48]. Measuring through the skin would remove the need for taking a blood sample, thus increasing patient comfort. A finger-prick device is an often used tool by diabetic patients to check their blood sugar levels. This device takes blood from the dermis, which is the layer of skin situated below the surface of the skin. Depending on the location of the body, the dermis can be 1 to 4 mm thick. This would mean that the LAD of the instrument would be large enough to reach the dermis in certain parts of the body. Furthermore, the same method might help detect other substances such as cholesterol or plaque build-up in arteries relatively close to the skin. The influence of the skin on the collected reflectance spectra could be removed by calibrating tissue near the artery.

# 7

# Conclusion

This thesis reported on the development of an instrument capable of guiding drilling into the pedicle during spinal surgery through diffuse reflectance spectroscopy (DRS). Throughout this report, it was investigated how optical fibres must be configured and integrated into an prototype to obtain directional feedback from inside a pedicle. Monte Carlo simulations were used to simulate light propagation through bone tissue to study the look-ahead distances in cancellous bone for core-to-core distances larger than 1 mm. The simulations showed that for core-to-core distances above 1 mm, the LAD increases as well, to a distance of 3.0 mm for a core-to-core distance of 4 mm. A larger LAD provides more time for the instrument user to react to the provided feedback and is therefore beneficial. An experiment verified the LAD simulations by conducting DRS measurements on an optical bone phantom.

A modular design was used to facilitate assembly. The prototype was made out of four components. The tip of the device houses the optical fibres. A frontal and sideways fibre pair were incorporated as this provides the instrument with independent sensing capability to both the side and front of the device. The body holds the fibre tubing and a connector is used to assemble all parts together.

The prototype is capable of detecting a cortical boundary at a minimum distance of 3.2 mm in front of the instrument, while the minimal look-ahead distance in a transverse direction was 1.2 mm. Combined with a rotating motion, reflectance data of the tissue volume surrounding the instrument can be obtained and thus detect the surrounding cortical wall inside the pedicle. In conclusion, this instrument is able to provide directional feedback based on the sensed distance to the cortical walls.

# Bibliography


[1] *Spine surgery | global trends  opportunities 2018 - life science intelligence 2022*. [Online]. Available: https://www.lifesciencemarketresearch.com/market-reports/spine-surgery-global-trends-opportunities-procedure-volumes-analysis-2018.

[2] A. Chan, E. Parent, K. Narvacan, C. San, and E. Lou, "Intraoperative image guidance compared with free-hand methods in adolescent idiopathic scoliosis posterior spinal surgery: A systematic review on screw-related complications and breach rates," *The Spine Journal*, vol. 17, no. 9, pp. 1215–1229, 2017, ISSN: 1529-9430. DOI: https://doi.org/10.1016/j.spinee.2017.04.001.

[3] A. Swamy, G. Burström, J. W. Spliethoff, D. Babic, C. Reich, J. Groen, E. Edström, A. Elmi Terander, J. M. Racadio, J. Dankelman, and B. H. W. Hendriks, "Diffuse reflectance spectroscopy, a potential optical sensing technology for the detection of cortical breaches during spinal screw placement," *Journal of Biomedical Optics*, vol. 24, no. 01, p. 1, Jan. 2019, ISSN: 1083-3668. DOI: 10.1117/1.JBO.24.1.017002.

[4] *Anatomy*, 2009. [Online]. Available: http://www.spinesurgery.co.in/anatomy.html.

[5] *Spinal cord*, 2022. [Online]. Available: my.clevelandclinic.org/health/body/21946-spinal-cord.

[6] *Transverse process definition*, 2022. [Online]. Available: https://www.spine-health.com/glossary/transverse-process.

[7] R. Droual, *Vertebral column*, 2022. [Online]. Available: http://droualb.faculty.mjc.edu/Lecture%20Notes/Fall%202007%20revisions%20to%20Anatomy%20notes/Vertebral%20Column%20with%20figures.htm.

[8] *Intervertebral disc*, 2022. [Online]. Available: https://www.physio-pedia.com/Intervertebral_disc.

[9] *Spinal instability: Causes and treatments*, 2022. [Online]. Available: https://www.hrosm.com/spinal-instability-causes-and-treatments/.

[10] B. C. Hospital, *Spinal fusion surgery*. 2022. [Online]. Available: https://www.childrenshospital.org/treatments/spinal-fusion-surgery.

[11] G. Choi, C. S. Pophale, B. Patel, and P. Uniyal, "Endoscopic spine surgery," *Journal of Korean Neurosurgical Society*, vol. 60, no. 5, pp. 485–497, Sep. 2017, ISSN: 2005-3711, 1598-7876. DOI: 10.3340/jkns.2017.0203.004.

[12] P. Hitchon, M. Brenton, J. Coppes, A. From, and J. Torner, "Factors affecting the pullout strength of self-drilling and self-tapping anterior cervical screws," *Spine*, vol. 28, pp. 9–13, Jan. 2003. DOI: 10.1097/01.BRS.0000038185.73138.CB.

[13] J. Weinstein, B. Rydevik, and W. Rauschning, "Anatomic and technical considerations of pedicle screw fixation," English (US), *Clinical Orthopaedics and Related Research*, vol. 284, pp. 34–46, 1992, ISSN: 0009-921X. DOI: 10.1097/00003086-199211000-00006.

[14] T. M. Shea, J. Laun, S. A. Gonzalez-Blohm, J. J. Doulgeris, W. E. Lee, K. Aghayev, and F. D. Vrionis, "Designs and techniques that improve the pullout strength of pedicle screws in osteoporotic vertebrae: Current status," *BioMed Research International*, vol. 2014, e748393, Mar. 2014, ISSN: 2314-6133. DOI: 10.1155/2014/748393.

[15] A. Swamy, "Breach detection using diffuse reflectance spectroscopy during spinal screw placement," Ph.D. dissertation, Delft University of Technology, 2021.

[16] T. Mattei, M. Meneses, J. Milano, and R. Ramina, "Free-hand technique for thoracolumbar pedicle screw instrumentation: Critical appraisal of current "state-of-art"," *Neurology India*, vol. 57, no. 6, p. 715, 2009, ISSN: 0028-3886. DOI: 10.4103/0028-3886.59465.

[17] I. D. Gelalis, N. K. Paschos, E. E. Pakos, A. N. Politis, C. M. Arnaoutoglou, A. C. Karageorgos, A. Ploumis, and T. A. Xenakis, "Accuracy of pedicle screw placement: A systematic review of prospective in vivo studies comparing free hand, fluoroscopy guidance and navigation techniques," *European Spine Journal: Official Publication of the European Spine Society, the European Spinal Deformity Society, and the European Section of the Cervical Spine Research Society*, vol. 21, no. 2, pp. 247–255, Feb. 2012, ISSN: 1432-0932. DOI: 10.1007/s00586-011-2011-3.

[18] N. Luther, J. B. Iorgulescu, C. Geannette, H. Gebhard, T. Saleh, A. J. Tsiouris, and R. Härtl, "Comparison of navigated versus non-navigated pedicle screw placement in 260 patients and 1434 screws: Screw accuracy, screw size, and the complexity of surgery.," *Journal of spinal disorders techniques*, vol. 28, no. 5, E298–303, Jun. 2015, ISSN: 1539-2465 1536-0652. DOI: 10.1097/BSD.0b013e31828af33e.

[19] A. Mason, R. Paulsen, J. Babuska, S. Rajpal, S. Burneikiene, E. Nelson, and A. Villavicencio, "The accuracy of pedicle screw placement using intraoperative image guidance systems: A systematic review," *Journal of Neurosurgery: Spine*, vol. 20, no. 2, pp. 196–203, 2014, ISSN: 15475654 (ISSN). DOI: 10.3171/2013.11.SPINE13413.

[20] R. Härtl, K. S. Lam, J. Wang, A. Korge, F. Kandziora, and L. Audigé, "Worldwide survey on the use of navigation in spine surgery," *World Neurosurgery*, vol. 79, no. 1, pp. 162–172, Jan. 2013, ISSN: 18788750. DOI: 10.1016/j.wneu.2012.03.011.

[21] L. Kobayashi Frisk, *Diffuse Reflectance Spectroscopy*, ser. Using a Monte-Carlo method to determine chromophore concentrations of tissue. 2016. [Online]. Available: https://lup.lub.lu.se/luur/download?func=downloadFile&recordOId=8882554&fileOId=8887864.

[22] S. Stolik, A. De la Cadena, and J. de la Rosa, "A diffuse reflectance spectroscopy system to study biological tissues," *Proc SPIE*, vol. 8785, Nov. 2013. DOI: 10.1117/12.2026477.

[23] *What-is-spectroscopy*, 2022. [Online]. Available: https://www.pasco.com/products/guides/what-is-spectroscopy.

[24] S. Koning, E. Baltussen, B. Karakullukcu, B. Dashtbozorg, L. Smit, R. Dirven, B. Hendriks, H. Sterenborg, and T. Ruers, "Toward complete oral cavity cancer resection using a handheld diffuse reflectance spectroscopy probe," *Journal of Biomedical Optics*, vol. 23, p. 1, Oct. 2018. DOI: 10.1117/1.JBO.23.12.121611.

[25] F. Fanjul-Vélez, S. Pampín-Suárez, and J. L. Arce-Diego, "Application of classification algorithms to diffuse reflectance spectroscopy measurements for ex vivo characterization of biological tissues," *Entropy*, vol. 22, no. 7, p. 736, 2020. DOI: 10.3390/e22070736.

[26] M. Duperron, K. Grygoryev, G. Nunan, C. Eason, J. Gunther, R. Burke, K. Manley, and P. O'brien, "Diffuse reflectance spectroscopy-enhanced drill for bone boundary detection," *Biomedical Optics Express*, vol. 10, no. 2, p. 961, Feb. 2019, ISSN: 2156-7085, 2156-7085. DOI: 10.1364/BOE.10.000961.

[27] G. Burström, A. Swamy, J. W. Spliethoff, C. Reich, D. Babic, B. H. W. Hendriks, H. Skulason, O. Persson, A. Elmi Terander, and E. Edström, "Diffuse reflectance spectroscopy accurately identifies the pre-cortical zone to avoid impending pedicle screw breach in spinal fixation surgery," *Biomedical Optics Express*, vol. 10, no. 11, p. 5905, Nov. 2019, ISSN: 2156-7085, 2156-7085. DOI: 10.1364/BOE.10.005905.

[28] W. Li, Y. Liu, and Z. Qian, "Determination of detection depth of optical probe in pedicle screw measurement device," *BioMedical Engineering OnLine*, vol. 13, no. 1, p. 148, Nov. 2014, Copyright license: https://creativecommons.org/licenses/by/4.0/, ISSN: 1475-925X. DOI: 10.1186/1475-925X-13-148.

[29] M. Epstein, "Fiber optics in medicine.," *Critical reviews in biomedical engineering*, vol. 7, no. 2, pp. 79–120, 1982.

[30] R. Paschotta, *Optical fiber communications*, 2008.

[31] Thorlabs, "0.22 na tecs double-clad, step-index, high power multimode fibe," *Thorlabs Specsheet*, Apr. 2019.

[32] *Image of lumbar vertebra*, 2022. [Online]. Available: http://smart.servier.com.

[33] S. H. Zhou, I. D. McCarthy, A. H. McGregor, R. R. H. Coombs, and S. P. F. Hughes, "Geometrical dimensions of the lower lumbar vertebrae - analysis of data from digitised ct images," *European Spine Journal*, vol. 9, no. 3, pp. 242–248, Jun. 2000, ISSN: 0940-6719, 1432-0932. DOI: 10.1007/s005860000140.

[34] M. Gstoettner, R. Lechner, B. Glodny, M. Thaler, and C. Bach, "Inter- and intraobserver reliability assessment of computed tomographic 3d measurement of pedicles in scoliosis and size matching with pedicle screws," *European spine journal: official publication of the European Spine Society, the European Spinal Deformity Society, and the European Section of the Cervical Spine Research Society*, vol. 20, pp. 1771–9, Jul. 2011. DOI: 10.1007/s00586-011-1908-1.

[35] N. Bertollo and W. R. Walsh, "Drilling of bone: Practicality, limitations and complications associated with surgical drill-bits," in *Biomechanics in Applications*, V. Klika, Ed., Rijeka: IntechOpen, 2011, ch. 3. DOI: 10.5772/20931. [Online]. Available: https://doi.org/10.5772/20931.

[36] A. Swamy, J. W. Spliethoff, G. Burstrom, D. Babic, C. Reich, J. Groen, E. Edstrom, A. Elmi-Terander, J. M. Racadio, J. Dankelman, and B. H. W. Hendriks, "Diffuse reflectance spectroscopy for breach detection during pedicle screw placement: A first in vivo investigation in a porcine model," *BioMedical Engineering OnLine*, vol. 19, no. 1, p. 47, Dec. 2020, ISSN: 1475-925X. DOI: 10.1186/s12938-020-00791-2.

[37] I. Krasnikov, A. Seteikin, and B. Roth, "Advances in the simulation of light–tissue interactions in biomedical engineering," *Biomedical Engineering Letters*, vol. 9, no. 3, pp. 327–337, Jul. 2019, ISSN: 2093-9868. DOI: 10.1007/s13534-019-00123-x.

[38] Q. Fang and D. A. Boas, "Monte carlo simulation of photon migration in 3d turbid media accelerated by graphics processing units," *Optics express*, vol. 17, no. 22, pp. 20 178–20 190, Oct. 2009, ISSN: 1094-4087.

[39] D. Marti, R. Aasbjerg, P. E. Andersen, and A. K. Hansen, "Mcmatlab: An open-source user-friendly matlab-integrated 3d monte carlo light transport solver with heat diffusion and tissue damage," in *Optical Interactions with Tissue and Cells XXX*, vol. 10876, International Society for Optics and Photonics, Mar. 2019, 108760T. DOI: 10.1117/12.2507754. [Online]. Available: https://www.spiedigitallibrary.org/conference-proceedings-of-spie/10876/108760T/MCmatlab--an-open-source-user-friendly-MATLAB-integrated-3D/10.1117/12.2507754.short.

[40] M. Uyuklu, M. Canpolat, H. J. Meiselman, and O. K. Baskurt, "Wavelength selection in measuring red blood cell aggregation based on light transmittance," *Journal of Biomedical Optics*, vol. 16, no. 11, pp. 1–10, 2011. DOI: 10.1117/1.3652712. [Online]. Available: https://doi.org/10.1117/1.3652712.

[41] G. T. Georgiev and J. J. Butler, "Long-term calibration monitoring of spectralon diffusers brdf in the air-ultraviolet," *Appl. Opt.*, vol. 46, no. 32, pp. 7892–7899, Nov. 2007. DOI: 10.1364/AO.46.007892. [Online]. Available: http://opg.optica.org/ao/abstract.cfm?URI=ao-46-32-7892.

[42] M. Yadlowsky, M. J. Papac, and B. Lassalas, *Illuminated microsurgical instrument including optical fiber with beveled end face*, 2014-11-26. [Online]. Available: https://patents.google.com/patent/US9561085B2/en?oq=US+patent+US+9561085+B2.+2017+2014%5C%2f11%5C%2f26..

[43] U. Silica, *Uv vs. ir grade fused silica | edmund optics*, 2022. [Online]. Available: https://www.edmundoptics.eu/knowledge-center/application-notes/optics/uv-vs.-ir-grade-fused-silica/.

[44] V. Gkatzidou, J. Giacomin, and L. Skrypchuk, "25. harris profile," in *Automotive Human Centred Design Methods*. De Gruyter, 2021, pp. 80–83. DOI: doi:10.1515/9783110677515-026. [Online]. Available: https://doi.org/10.1515/9783110677515-026.

[45] K. A. Houpt, T. R. Houpt, and W. G. Pond, "The pig as a model for the study of obesity and of control of food intake: A review," *The Yale Journal of Biology and Medicine*, vol. 52, no. 3, pp. 307–329, 1979, ISSN: 0044-0086.

[46] A. F. Samdani, M. Djurasovic, S. I. Bailey, C. Brown, J. Asghar, L. P. D'Andrea, J. Dimar, H. L. Shufflebarger, and J. Gaughan, "Pediguard: A solution for the challenges of pedicle screw placement," p. 8,

[47] J. Williams, A. Samdani, H. L. A. Defino, K. George, J. Gaughan, and R. Betz, "Anticipation of vertebral pedicle breach through dynamic surgical guidance," *Coluna/Columna*, vol. 13, no. 3, pp. 210–213, Sep. 2014, ISSN: 1808-1851. DOI: 10.1590/S1808-18512014130300R85.

[48] B. Javid, F. Fotouhi-Ghazvini, and F. S. Zakeri, "Noninvasive optical diagnostic techniques for mobile blood glucose and bilirubin monitoring," *Journal of Medical Signals and Sensors*, vol. 8, no. 3, pp. 125–139, 2018, ISSN: 2228-7477. DOI: 10.4103/jmss.JMSS_8_18.